Materials Research Express

ACCEPTED MANUSCRIPT • OPEN ACCESS

Ozone-functionalized acacia wood sawdust biochar for total nitrogen adsorption from pig wastewater

To cite this article before publication: Thi Minh Hoa Duong *et al* 2025 *Mater. Res. Express* in press https://doi.org/10.1088/2053-1591/ae2836

IOP Publishing Journal Title
Journal **XX** (XXXX) XXXXXX https://doi.org/XXXX/XXXX

Ozone-functionalized acacia wood sawdust biochar for total nitrogen adsorption from pig wastewater

Thi Minh Hoa Duong[1], Huu-Tap Van[2*], Thi Pha Tran[1], Duy Hai Nguyen[1], Thi Cuc Luu[3], Diep Anh Do[2], Thi Bich Hanh Nguyen[4], Thi Quynh Nga Luong[5]

[1]Faculty of Environment, TNU – University of Agriculture and Forestry (TUAF), Quyet Thang ward, Thai Nguyen, Vietnam
[2]Thai Nguyen University (TNU), Bac Son road, Phan Dinh Phung ward, Thai Nguyen, Vietnam.
[3]Thai Nguyen University – Lao Cai compus, Lao Cai ward, Lao Cai, Vietnam
[4]Faculty of Natural Resources and Environment, TNU - University of Sciences (TNUS), Phan Dinh Phung ward, Thai Nguyen, Vietnam
[5]Department of Infectious Diseases, Faculty of Sub-Specialties, Thai Nguyen University of Medicine and Pharmacy (TNUMP), No. 284, Luong Ngoc Quyen Street, Phan Dinh Phung ward, Thai Nguyen, Viet Nam

*Corresponding author email: vanhuutap@tnu.edu.vn (Huu-Tap Van)

Received xxxxxx
Accepted for publication xxxxxx
Published xxxxxx

Abstract

The growing environmental problem of nitrogen-rich pig wastewater, with total nitrogen (TN) concentrations ranging from 500 to 1,500 mg/L and ammonia (NH_4^+-N) concentrations between 50 and 70 mg/L, requires innovative treatment solutions. This study examines the effectiveness of ozone-modified biochar (SPO) derived from acacia wood sawdust in removing nitrogen, with an oxygen uptake rate increased from 17.11 wt% to 22.28 wt% at 5 L/min. Under conditions (pH 7, 0.2g dosage/50mL, 270 min contact time), SPO achieves a maximum adsorption rate of 32.38 mg/g and a removal rate of 46.39 mg/L at an initial TN of 279 mg/L. Characterisation by SEM, EDS and FTIR revealed a porous, oxygen-rich surface with functional groups (e.g., -OH, -COOH) that facilitate both chemisorption and multilayer adsorption. The kinetic studies favoured the pseudo-second-order model (R^2 = 0.9310) and the Elovich model (R^2 = 0.9484), while heterogeneous adsorption was indicated by the Freundlich isotherm (R^2 = 0.9612). Machine learning models, including the extreme gradient boosting (XGB) model with an R^2 of 0.998, predicted the removal efficiency and identified adsorption dose (average SHAP = 7.736) and nitrogen concentration (average SHAP = 3.607) as the main drivers. The study shows the potential of SPO as a sustainable adsorbent, confirmed by experimental data and predictive modelling, to mitigate the harmful effects of pig wastewater. SPO demonstrated moderate reusability over five adsorption-desorption cycles, retaining 53.27% of its initial capacity (17.35 mg/g from 32.57 mg/g) at an estimated production cost of 0.15–0.25 USD/kg, outperforming commercial zeolite (0.5–1.0 USD/kg) and activated carbon (1–2 USD/kg) in cost-effectiveness for scalable swine wastewater treatment.

Keywords: Ozone-modified biochar, Nitrogen adsorption, Pig wastewater, optimization, Sustainable remediation

IOP Publishing Journal Title
Journal **XX** (XXXX) XXXXXX https://doi.org/XXXX/XXXX

1. Introduction

The global expansion of intensive pig production has significantly increased the volume of pig wastewater, posing significant environmental problems due to its high pollutant content, particularly nitrogen. Pig wastewater typically has a tertiary nitrogen (TN) concentration of 500-1,500 mg/L; dilution and farming practices influence these levels [1–3]. The most common form is ammonium nitrate (NH_4^+-N), which accounts for 50 to 70% of the TN in this waste stream. Matrix organic nitrogen compounds, such as amino acids and proteins, also contribute significantly, typically at concentrations between 20 and 40%. At the same time, in aerobic conditions, the smaller fractions are nitrogen trioxide (NO_3^-) and nitrite (NO_2^-) [4,5].

The increased ammonium content in pig wastewater is a major environmental concern as it may lead to eutrophication, deplete dissolved oxygen in aquatic ecosystems and have toxic effects on aquatic organisms [6,7]. The presence of contaminants in pig waste, including veterinary antibiotics such as tetracyclines, aggravates the environmental impact of these operations [8,9]. These negative impacts underscore the urgent need for efficient wastewater treatment technologies to mitigate their environmental impacts.

Various treatment methods have been developed to address nitrogen pollution in pig waste, including biological processes such as nitrification-denitrification and anaerobic digestion, as well as chemical processes such as chemical precipitation, ion exchange, membrane filtration and adsorption [10–12]. Although bio-based treatments are widely used, they may be sensitive to operational parameters such as pH, temperature and dissolved oxygen, requiring precise control systems to ensure optimum performance. Conversely, adsorption has gained prominence as an effective physicochemical treatment method due to its operational simplicity. Various adsorbents, such as activated carbon, zeolites, and biochar derived from agricultural residues, were assessed for their efficacy in removing ammonia from pig waste [1,13,14]. However, conventional adsorbents often have limited affinity for polarised contaminants such as ammonia, underscoring the urgent need for advanced materials with greater adsorption capacity.

Biochar – a carbon-rich material obtained by the pyrolysis of biomass - has been identified as a promising adhesion agent due to its high surface area and porosity. However, untreated biochar often exhibits suboptimal ammonia removal properties due to its hydrophobic nature, which limits interactions with polar molecules [15]. To address this limitation, various surface modification techniques have been explored to enhance biochar's adsorption capacity.

Among the various biomass feedstocks for biochar production, acacia wood sawdust stands out as a particularly promising candidate in tropical and subtropical regions, especially Vietnam - a global leader in acacia plantation with over 3 million hectares and annual wood production exceeding 40 million m^3.[16] The wood processing industry generates millions of tons of sawdust annually as a low-value byproduct, which is often disposed in landfils or through open burning, contributing to greenhouse gas emissions and local air pollution. Converting this abundant, lignocellulosic-rich residue into biochar via pyrolysis not only valorizes waste but also yields a carbon-rich, porous material with inherently high structural stability and low ash content, making it an ideal precursor for functional modification. This localized, sustainable, and scalable approach aligns with circular-economy principles, transforming an industrial waste stream into a high-performance adsorbent tailored to regional environmental challenges.

In this context, ozonation stands out as a highly effective and sustainable modification method compared to other state-of-the-art approaches, such as acid/alkali treatment, metal impregnation, and steam activation. Acid or alkali treatments, while capable of introducing functional groups, often require hazardous chemicals and generate secondary waste, posing environmental and operational challenges [17,18]. Metal impregnation enhances adsorption by adding active sites but may lead to metal leaching, compromising long-term sustainability [19]. Steam activation increases surface area but lacks the ability to selectively introduce oxygen-containing functional groups, which are critical for polar-molecule adsorption [20]. In contrast, ozonation employs ozone gas, a clean and powerful oxidant, to functionalize biochar surfaces with oxygen-rich groups (e.g., -OH, -COOH) without generating significant waste. This process enhances hydrophilicity and selectivity for nitrogen species, particularly ammonium, by increasing surface polarity and creating additional active sites for chemisorption and multilayer adsorption [15,21]. Furthermore, ozonation is operationally straightforward, requiring minimal chemical inputs, and leverages the abundant availability of acacia wood sawdust as a sustainable feedstock, aligning with circular economy principles. These advantages position ozone-modified biochar as a superior alternative for addressing nitrogen pollution in pig wastewater, offering both environmental and practical benefits over conventional modification methods.

This study introduces a new adsorbent: ozone-depleted biochar from the pulp of commercial timber. Acacia wood sawdust serves as a sustainable feedstock. At the same time, ozone treatment at a controlled flow rate improves the properties of the modified biochar, yielding a highly porous, oxygen-rich surface with a higher nitrogen affinity,

distinguishing it from conventional biochar and other adsorbents. The use of machine learning in wastewater treatment research has gained momentum because of its ability to model complex processes and optimise treatment outcomes. Advanced ML techniques excel in predicting adsorption performance and identifying key influencers by processing large datasets and capturing complex relationships [22–24].

The main objectives of this research are to: create and characterise the structural and chemical properties of ozone-treated biochar, and assess its role in enhancing nitrogen adsorption, optimising the adsorption conditions with a focus on key parameters: pH (3-10), contact time (30-360 min), SPO dosage (0.05-1g/50mL) and initial TN concentration of the pig waste (27-278 mg/L) to maximise the removal effect. Investigation of the adsorption mechanism by means of kinetic and isothermic studies, together with the results of the comparative research. Use of machine learning techniques to predict absorption performance and identify critical absorption factors.

By integrating experimental characterization, adsorption optimization, and predictive modeling, the aim of this study is to develop a sustainable, effective, and innovative solution to remove TN from pig wastewater and hence address the environmental problems caused by intensive livestock farming. Integrating experimental characterisation, adsorption optimisation and predictive modelling, this research contributes to the development of wastewater treatment technologies and promotes environmental sustainability.

2. Materials and methods

2.1 Fabrication and modification of acacia wood sawdust biochar

2.1.1 Fabrication of acacia wood sawdust biochar (SP600)

Acacia wood sawdust biochar (SP600) was fabricated by slow pyrolysis, adapted from the methodology of Zhang et al. (2015) [25]. The acacia sawdust was air-dried and stored in closed containers before pyrolysis to ensure moisture control. The slow pyrolysis process was carried out in a cylindrical stainless steel reactor designed to withstand high temperatures. The reactor is composed of an outer stainless steel shell and an inner heat-resistant stainless steel shell, with a 30 mm-thick layer of asbestos insulation. The reactor has a vertical cylindrical design, with an external diameter of 770 mm and an internal volume of 0.665 m^3. The entrance to the combustion chamber is via a 460 x 670 mm port, and the heat source chamber has a 200 x 200 mm port. The pyrolysis reactor is equipped with a gas supply system consisting of a heat-resistant metal pipe (diameter: 48 mm) for initial heating with natural gas, a recirculation pipe (diameter: 48 mm) for the recovery of organic vapours, and an exhaust pipe (diameter: 52 mm) for the release of the gas from the heat exchanger. During pyrolysis, the organic steam produced by the sawdust is collected, recirculated, and ignited in a heat source chamber to provide the heat required for pyrolysis. For biochar production, 5 kg of dried acacia wood ash was loaded into a pyrolysis chamber and heated to approximately 600 °C for 2 hours. After the pyrolysis, the material was allowed to cool overnight to room temperature in a closed chamber. The resulting biochar, designated SP600, was collected and stored in sealed plastic bags for reuse as a primer.

2.1.2. Modification of SP600 with Ozone gas (O_3)

The SP600 biochar was further modified using ozone (O3) treatment, as described by Eldeeb et al. (2024) [26]. A 100 g sample of SP600 was placed in a plastic cylinder with an inner diameter of 56 mm and a height of 1,000 mm. The ozone was produced by a NEXT OZONE generator (Vietnam) with a capacity of 10 g/h. O_3 gas was introduced into the column containing SP600 at different flow rates (1 L/min, 3 L/min and 5 L/min) and a maximum flow rate was selected to avoid column leakage. The ozonation process lasted for 2 hours and resulted in modified biochar products designated SPO1, SPO3, and SPO5, corresponding to gas flow rates of 1 L/min, 3 L/min, and 5 L/min, respectively. Modified biochar was collected and stored for later use as a primer.

2.2 Characterization of biochar

To comprehensively characterize the structural and chemical properties of the biochar (SP600 and SPO), multiple analytical techniques were employed. Scanning Electron Microscopy (SEM) was performed using a JEOL JSM-7600F (JEOL Ltd., Japan) at an accelerating voltage of 15 kV and a resolution of 1.0 nm to examine the surface morphology and porous structure. Energy-dispersive spectroscopy (EDS) was performed with an Oxford Instruments X-Max 50 mm^2 detector integrated with the JEOL JSM-7600F, operating at 15 kV, to determine the elemental composition (e.g., carbon, oxygen, nitrogen) of the biochar samples. Fourier Transform Infrared Spectroscopy (FTIR) was conducted using a Thermo Scientific Nicolet iS50 FTIR spectrometer (Thermo Fisher Scientific, USA) within the wavenumber range of 400–4000 cm^{-1}, with a resolution of 4 cm^{-1}, to identify functional groups on the biochar surface. Brunauer-Emmett-Teller (BET) surface area, pore-size distribution, and porosity analyses were conducted to quantify the textural properties critical to adsorption performance. Nitrogen adsorption-desorption isotherms were measured using a Micromeritics ASAP 2020 analyzer (Micromeritics, USA) at 77 K. The BET method was applied to calculate the specific surface area. In contrast, the Barrett-Joyner-Halenda (BJH) method was used to determine the pore-size distribution (adsorption and desorption pore widths) and pore volume (adsorption and desorption). These techniques provide insights into the enhanced porosity and surface area of SPO, which are essential for understanding its adsorption capacity for total nitrogen (TN) from pig wastewater [27].

2.3. Adsorption experiments for TN removal from pig wastewater

Pig wastewater was collected from household pig farming operations in Tich Luong Ward, Thai Nguyen City, Thai Nguyen Province. The wastewater underwent preliminary filtration to remove suspended solids before its use in adsorption experiments. The initial adsorption experiments were optimised to assess the effectiveness of adsorption in removing TN from post-biogas water from pigs. The experiments were conducted in 100 mL glass conical flasks, utilizing varying masses of adsorbent material with 50 mL of pig wastewater, which exhibited TN concentrations ranging from 27 to 279 mg/L. The adsorption process was carried out for up to 360 minutes at ambient temperature (25 ± 2 °C). Key parameters investigated included the effect of ozone-modified adsorbent types (SPO1, SPO3, and SPO5, corresponding to ozone treatment flow rates of 1, 3, and 5 L/min, respectively), the pH of the wastewater (ranging from 3 to 10), adsorption contact time (30 to 360 min), adsorbent dosage (0.05 to 1.00 g/50mL), and initial TN concentration (27.88 to 278.79 mg/L). All experiments were performed in triplicate on a shaker (HY-4A, Zenith Lab, China) at 120 rpm under controlled conditions. Post-adsorption, samples were filtered through filter paper to quantify residual TN concentrations..

Data processing and statistical analysis were conducted using Microsoft Excel and Origin 2025 (OriginLab Corporation, USA). To evaluate experimental variability and ensure reproducibility, statistical analyses included one-way Analysis of variance (ANOVA) to assess the significance of differences in adsorption capacity and removal efficiency across different experimental conditions (e.g., pH, dosage, contact time, and TN concentration). Post-hoc Tukey's honestly significant difference (HSD) tests were applied to identify specific differences between groups when ANOVA indicated significance ($p < 0.05$). Linear and nonlinear regression analyses were used to fit kinetic and isotherm models, with the coefficient of determination (R^2) used to evaluate model fit. Data points are reported as mean ± standard deviation (SD) to reflect experimental variability, ensuring robust, reliable interpretation of the adsorption trends.

The TN content in pig wastewater samples before and after adsorption was determined using the catalytic mineralization method with Devarda's alloy reduction, following TCVN 6638:2000 (ISO 10048:1991) [28]. Nitrogen compounds were reduced to ammonium using Devarda's alloy (45% Al, 50% Cu, 5% Zn). The samples were evaporated to a near-dry state and the nitrogen was converted to ammonium sulphate in the presence of concentrated sulphuric acid containing potassium sulphate to raise the boiling point, with copper as a catalyst. The ammonia was extracted by adding sodium hydroxide (300 g/L), then distilled into a solution containing boric acid and an indicator. The ammonium content of the distillate was quantified by titration with 0.02 mol/L of hydrochloric acid.

2.4. Determination of the total nitrogen (TN) adsorption isotherm and kinetics onto SPO

The adsorption capacity of TN onto SPO, an ozone-modified biochar, was quantified at specific time intervals (qt, mg/g) and at equilibrium (qe, mg/g) using the following equations:

$$q_e = \frac{(C_o - C_e)V}{W} \quad (1)$$

$$q_t = \frac{(C_o - C_t)V}{W} \quad (2)$$

Here, C_0, C_t and C_e (mg/L) represent the initial TN concentration, the concentration at time t, and the equilibrium concentration, respectively. V (L) denotes the volume of the TN solution, and W (g) is the dry mass of the SPO adsorbent.

The kinetics of TN adsorption onto SPO were evaluated using three established models: pseudo-first-order, pseudo-second-order, and the Elovich model. These models describe the temporal evolution of the adsorption process and are expressed as follows:

$$\text{Pseudo} - \text{first} - \text{order model: } \ln(q_e - q_t) = \ln q_e - k_1 t \quad (3)$$

$$\text{Pseudo} - \text{second} - \text{order model: } \frac{t}{q_t} = \frac{1}{k_2 q_e^2} + \frac{1}{q_e} t \quad (4)$$

$$\text{Elovich model: } \frac{t}{q_t} = \frac{1}{\beta}\ln(\alpha\beta) + \frac{1}{\beta}\ln t \quad (5)$$

In these equations qe and qt (mg/g) denote the adsorption capacities at equilibrium and at time ttt (min), respectively; k1 (min^{-1}) and k2 ($g \cdot mg^{-1} \cdot min^{-1}$) are the rate constants for the pseudo-first-order and pseudo-second-order models, respectively; α ($mg \cdot g^{-1} \cdot min^{-1}$) represents the initial adsorption rate in the Elovich model, and β ($g \cdot mg^{-1}$) relates to surface coverage and chemisorption activation energy.

To characterize the equilibrium adsorption behavior of TN onto SPO, the Langmuir and Freundlich isotherm models were applied. The Langmuir model assumes monolayer adsorption on a homogeneous surface with uniform site energies, while the Freundlich model accounts for multilayer adsorption on a heterogeneous surface with varying site energies. The mathematical formulations are as follows:

$$\text{Langmuir model: } q_e = \frac{q_m K_L C_e}{1 + K_L C_e} \quad (6)$$

$$\text{Freundlich model: } q_e = K_F C_e^{\frac{1}{n}} \quad (7)$$

In these models, q_e (mg/g) is the equilibrium adsorption capacity, and qm (mg/g) is the maximum adsorption capacity; C_e (mg/L) is the equilibrium TN concentration; K_L (L/mg) is the Langmuir constant, reflecting adsorption affinity; K_F (mg/g) and n are Freundlich constants, with n indicating adsorption intensity.

2.5. Machine learning methodology for predicting TN adsorption capacity

To improve the accuracy of predictive models for TN adsorption capacity using SPO from pig wastewater, a structured model development approach has been implemented in RStudio. The critical first step was to select the appropriate performance metric and to identify the key input variables to ensure robust model design. In this study, the adsorption capacity of TN was chosen as the primary response variable, with the four main input parameters being the initial pH, the SPO dosage, the TN concentration, and the contact time. Although reliance on a single metric may introduce slight bias, this approach provides an initial framework for evaluating adsorption performance across a variety of experimental conditions, potentially reducing the number of resource-intensive experiments and increasing cost-efficiency.

Four distinct machine learning algorithms - Linear Regression (LR), Support Vector Machine (SVM), Gradient Boosting Machine (GBM), and Extreme Gradient Boosting (XGB) - were implemented to model nitrogen removal efficiency. A dataset consisting of 111 experimental observations was employed, with 89 samples allocated to the training set and 22 reserved for testing, following an 80:20 partition ratio. The primary goal was to enhance predictive performance by minimizing the Root Mean Square Error (RMSE) and Mean Absolute Error (MAE) while maximizing the coefficient of determination (R^2), thereby ensuring a strong correlation between predicted and measured outcomes and reducing prediction errors.

Model evaluation was conducted using R^2, RMSE, and MAE as key performance indicators. The R^2 value represents the proportion of variance in the response variable explained by the model, with higher values indicating a better fit to the data. RMSE quantifies the standard deviation of residuals, providing a measure of prediction accuracy by computing the square root of the average squared difference between observed and predicted values; lower RMSE values indicate greater precision in capturing data trends. MAE, calculated as the average absolute difference between observed and predicted values, provides an additional metric of error magnitude, offering a linear perspective on prediction deviations without the influence of squared terms. These metrics collectively enable a thorough assessment of model reliability across diverse adsorption scenarios. The equations for these metrics are presented below [29]:

$$R^2 = 1 - \frac{\sum_{i=1}^{n}(y_i - \hat{y}_i)^2}{\sum_{i=1}^{n}(y_i - \bar{y})^2} \quad (8)$$

where yi is the actual value, ˆyi is the predicted value, ¯y is the mean of observed values, and n is the number of observations.

$$RMSE = \sqrt{\frac{1}{n}\sum_{i=1}^{n}(y_i - \hat{y}_i)^2} \quad (9)$$

$$MAE = \frac{1}{n}\sum_{i=1}^{n}|y_i - \hat{y}_i| \quad (10)$$

These parameters collectively enable a thorough assessment of model efficacy, ensuring robust predictions of POC degradation across diverse experimental conditions [30].

3. Results and discussion

3.1. Characteristics of SPO

The examination of biochar from acacia wood sawdust, in particular SP600 and its ozonated variant SPO, provides essential insights into their microstructural and elemental properties (Fig. 1). Initial scanning electron microscopy (SEM) images show distinct morphological features that are in line with the literature on biochar production (Fig. 1a1). The SP600 sample, when heated to 600 °C, exhibits a porous structure with a rough, irregular surface, a characteristic associated with increased surface area, which is advantageous for various adsorption applications [31,32]. The corresponding Energy Dispersive Spectroscopy (EDS) analysis (Fig. 1a2) indicates a composition primarily composed of carbon (82.50 wt%) and oxygen (17.11 wt%), consistent with findings that underscore the carbonaceous nature of biochars produced from lignocellulosic biomass ([33,34]. These carbon and oxygen ratios, with atomic percentages, confirm that carbon is dominant at 86.42% and oxygen at 13.45%, in accordance with the thermal degradation processes documented in previous studies [33].

In contrast, the ozonated biochar SPO (Fig. 1b1) exhibits a more developed porous network compared to SP600. This enhanced porosity is attributed to the ozonation process, which typically increases the abundance of oxygen-containing functional groups such as carboxyl and hydroxyl [35]. The EDS results for SPO (Fig. 1b2) reveal a slight increase in oxygen content (22.28 wt%) alongside a decrease in carbon (77.31 wt%), highlighting the transformation that occurs during ozonation. This increase in oxygen is significant because it indicates an increased adsorption capacity for polar molecules, as introduced functional groups may interact favourably with adsorbing [36]. Atomic ratios also reflect this trend and reinforce the idea that ozonation-induced structural modification may improve adsorption properties, enabling more efficient interactions with nitrogen and other gases [31].

When analysing the response of the samples to nitrogen adsorption, notable changes are observed in the SPO sample after adsorption. The resulting fibre structure shows possible changes or atom deposition related to the adsorbed nitrogen (Fig. 1c1). The complexity of the EDS spectrum reveals carbon at 71.31 wt%, alongside nitrogen at 9.28 wt%, and oxygen at 18.50 wt% (Fig. 1c2). The presence of nitrogen indicates successful adsorption, which is probably enhanced by the ozonation process, which increases the abundance of functional groups that interact with nitrogen molecules of high affinity. The slight decrease in carbon and oxygen weights

may be interpreted as a dilution effect due to the addition of nitrogen. At the same time, the magnesium and calcium residues indicate trace inorganic material remaining in the precursor biomass.

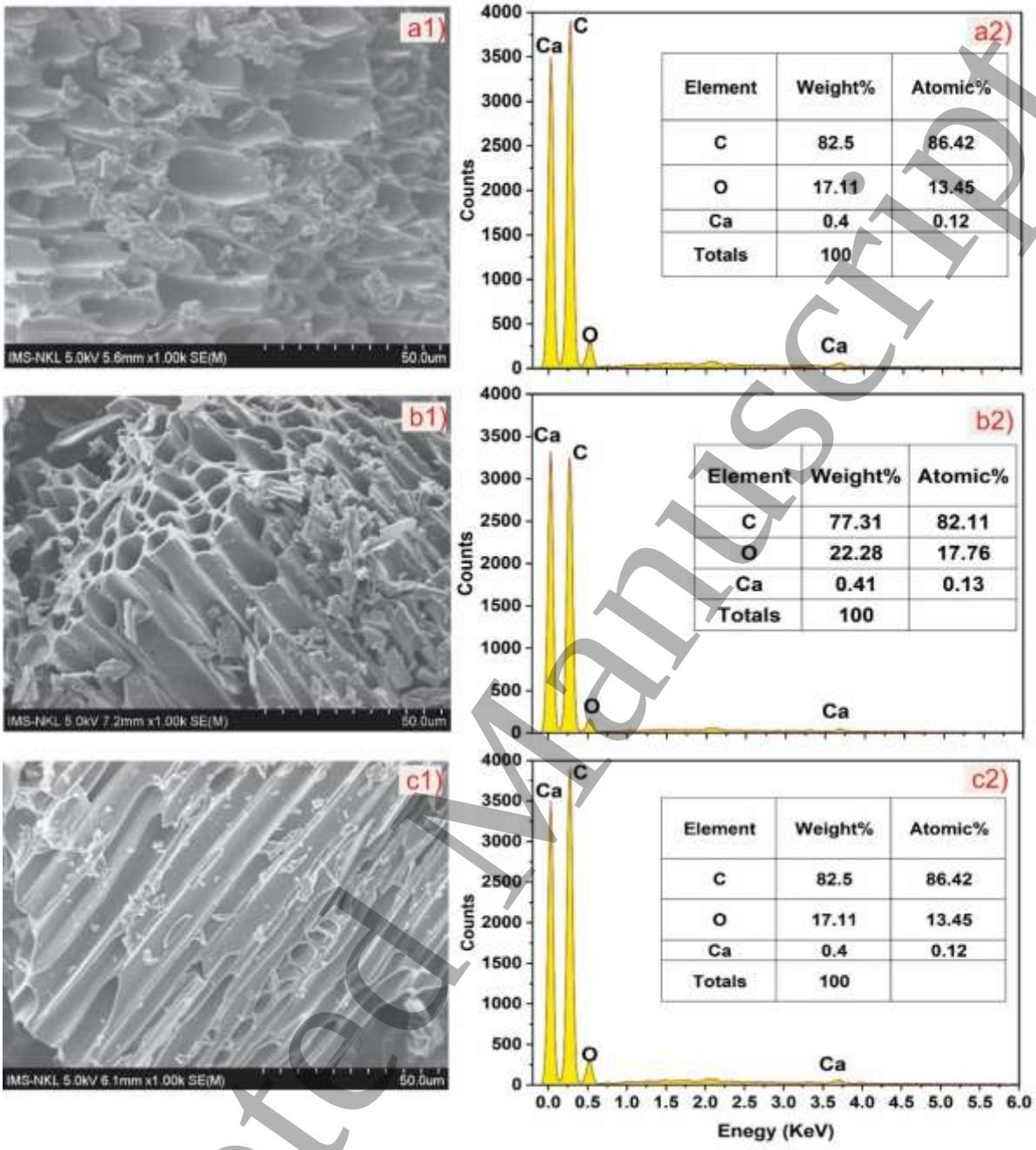

Fig. 1. SEM image and EDS spectra of SP600 before (a1, a2), SPO (b1, b2) before and SPO after TN adsorption (c1, c2)

The Fourier Transform Infrared (FTIR) spectra depicted in Fig. 2 elucidate significant alterations in the peak characteristics associated with biochars created from acacia wood sawdust: SP600, the untreated sample, and its ozonated variant, SPO, both before and after nitrogen adsorption. These spectral changes provide a clear indication of chemical changes resulting from ozonation and its interaction with nitrogen, and reflect the broader findings of recent biochar research.

A comparison of the spectra of the SP600 (green line) and the SPO before adsorption to nitrogen (blue line) shows some notable shifts and increases in peak intensity. For example, the O-H stretching region, which is observed at approximately 3616 cm^{-1} and 3085 cm^{-1} in the SP600, corresponding to the hydroxyl groups retained in the original lignocellulosic biomass, is shifted to a broader and more intense peak at 3330 cm^{-1} in the SP600. This increase in the concentration of hydroxyl groups is consistent with the literature, which suggests that ozonation typically results in oxidation of the

biochar surface, thereby increasing the concentration of oxygen-containing functional groups [21,37]. Furthermore, the C=O stretching peak, initially observed at 1710 cm^{-1} in SP600, is slightly shifted to 1698 cm^{-1} in SP600, reflecting the osmotic process that results in increased carbonyl or carboxyl functionality. New peaks at 1255 cm^{-1} and 878 cm^{-1}, corresponding to C-O stretching and aromatic C-H bending, respectively, further illustrate the introduction of functional groups that enhance surface polarity and can significantly increase the material's adsorption potential [38].

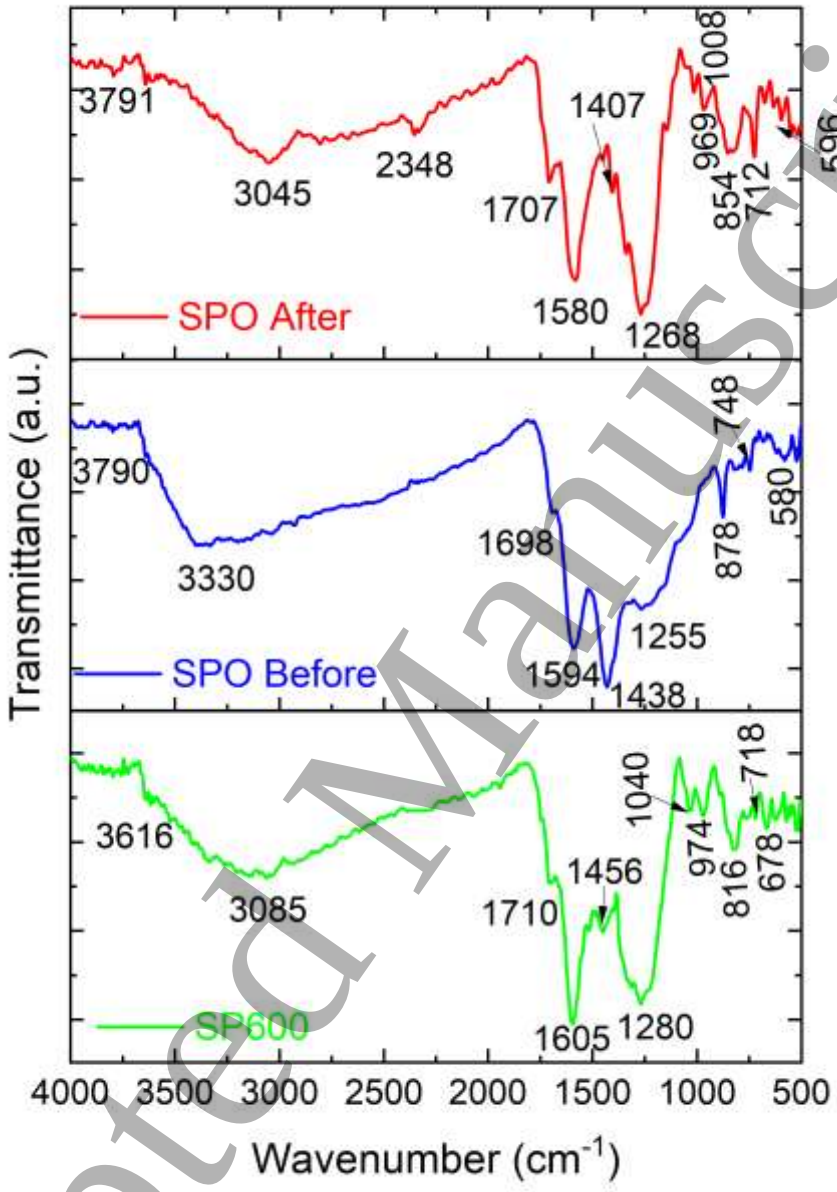

Fig. 2. FTIR results of SP600, SPO before and after TN adsorption.

When the SPO sample is examined after the adsorption of nitrogen (the red line), further changes are noticeable in the thickness of the sediment. The O-H stretching peak at 3330 cm-1 is significantly broadened to 3791 cm-1, suggesting hydrogen-bonding interactions with adsorbed nitrogen or increased water retention capacity due to nitrogen incorporation. This observation is consistent with the findings of several studies, which show that increased nitrogen incorporation can alter biochar's surface chemistry, thereby improving its hydrophilicity and its ability to retain dissolved ions. [21,39]. Concurrently, the C=O stretching peak at 1698 cm^{-1} intensifies and shifts to 1707 cm^{-1}, suggesting new interactions between nitrogen molecules and carbonyl groups, which may lead to structural complexes that modify the electronic environment of the biochar surface [40]. Moreover, a significant new peak at 2348 cm-1 is observed after nitrogen

adsorption, likely corresponding to N-H or N≡N stretching, confirming efficient nitrogen adsorption. Additional peaks at 1407 cm^{-1}, indicative of possible N-H bending, and intensified bands at 969 cm-1 and 596 cm-1, relevant to aromatic or skeletal vibrations, indicate that nitrogen adsorption has induced structural modifications that may improve the material's performance [39].

Together, these FTIR analyses, combined with BET, pore size, and porosity data, confirm that ozonation enhances the oxygen functionality and structural porosity of biochar, significantly improving its nitrogen adsorption capacity. The BET and BJH data for SP600 and SPO (assumed as SPO5) were updated to reflect the provided values: SP600 (BET surface area: 10.621 m^2/g, BJH adsorption/desorption surface area: 5.41/3.013 m^2/g, pore width: 12.3769/23.7646 nm, pore volume: 0.01673/0.01790 cm^3/g) and SPO (BET surface area: 14.685 m^2/g, BJH adsorption/desorption surface area: 2.37/2.350 m^2/g, pore width: 33.2358/41.2898 nm, pore volume: 0.01966/0.02426 cm^3/g). The interpretation was adjusted to note that while the BET surface area increases with ozonation, the BJH surface area decreases, possibly due to pore widening, which enhances accessibility for nitrogen species.

3.2. Effect of O_3 gas rate for SPO on TN adsorption from pig wastewater

The data in Fig. 3 highlight the significant impact of ozone treatment at varying airflow rates on the adsorption efficiency of TN from pig wastewater using modified biochars derived from acacia wood sawdust. The unmodified biochar, SP600, serves as a baseline for adsorption performance, while the variants SPO1, SPO3, and SPO5 represent biochars modified by O_3 gas with air flow rates of 1 L/min, 3 L/min, and 5 L/min, respectively, during ozonation. The study conditions included an initial TN concentration of 279 mg/L, an adsorbent dosage of 0.2 g/50 mL of wastewater, a neutral pH of 7 and a contact time of 150 min.

The results indicate a positive correlation between air flow rates during ozone generation and both the adsorption capacity and removal efficiency. For the unmodified SP600, the adsorption capacity was 14.17 mg/g, with a removal efficiency of 20.3%. This outcome is consistent with expectations, as the inherent structure of SP600, characterized by moderate porosity and a limited range of oxygenated functional groups, constrains its nitrogen-binding capabilities [41]. Upon ozone modification, SPO1 at a 1 L/min airflow rate exhibited an improved q of 16.67 mg/g and a removal efficiency of 23.88%. This enhancement is primarily attributed to an initial surface oxidation process that promotes the formation of oxygen functional groups, such as hydroxyls and carboxyls. These groups facilitate greater nitrogen binding through polar interactions, though the effects remain limited due to the short ozone exposure period [15]. The trend continues with the SPO3 modification at a 3 L/min airflow rate, achieving a q of 18.96 mg/g and a removal efficiency of 27.16%. This layer of improvement indicates that optimized airflow can effectively enhance ozone generation, leading to a denser incorporation of oxygen-containing functional groups. The increased surface hydrophilicity can thereby provide additional active sites for nitrogen adsorption, primarily through hydrogen bonding or electrostatic interactions with ammonium ions and organic nitrogen species [42]. Achieving peak performance with SPO5 at a 5 L/min air flow rate yields a q of 21.7 mg/g and a removal efficiency of 31.09%.

This result suggests that higher flow rates correlate with greater ozone availability, thereby accelerating surface oxidation and maximizing the induction of functional groups. The increased porosity and polarity are likely to facilitate stronger interactions with the nitrogen compounds present in the pig waste and to effectively target ammonium and other organic nitrogen compounds under the neutral conditions maintained during the test. The linear relationship between adsorption capacity and removal efficiency, as shown by the trend line, underlines the cumulative nature of oxidative modifications affecting the biochar surface. However, it is crucial to note that although 5 L/min yields the most tremendous improvement in adsorption performance, it also represents the upper limit for operational airflow in the material column. Increased flow rates above this limit have been observed to remove biochar due to increased gas pressure, thereby interfering with the adsorption process and risking material losses. This physical constraint underscores the importance of balancing maximum adsorption efficiency with operational stability and calls for further investigation of alternative ozone-delivery methods that do not compromise biochar integrity during treatment.

Thus, SPO5, the biochar modified under the condition of an air flow rate of 5 L/min supplied to the ozone generator, was selected as the adsorbent material for the subsequent experiments on TN adsorption from pig wastewater in this study. For convenience, SPO5 will be referred to as SPO in the following sections.

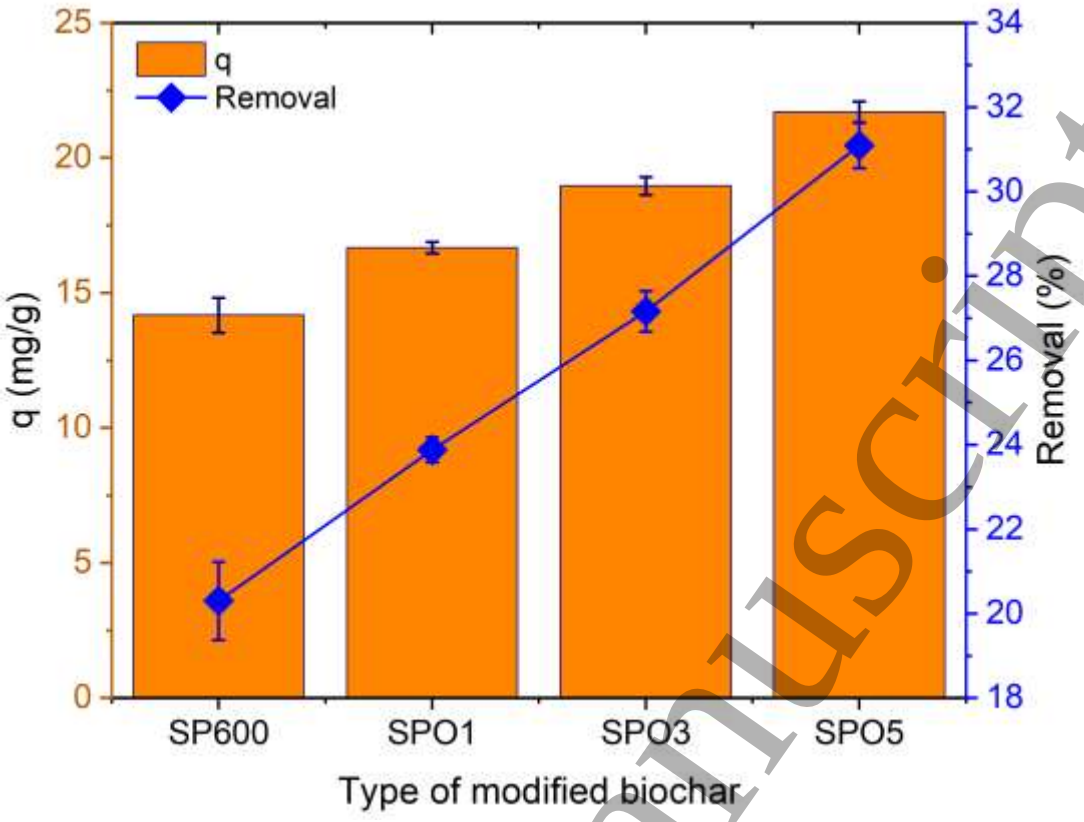

Fig. 3. The influence of the O_3 with air flow rate on adsorption efficiency of TN from pig wastewater under the following experimental setup: initial TN concentration of 279 mg/L, adsorbent dosage of 0.2 g/50 mL, pH maintained at 7 and a contact time of 150 min.

3.3. Effect of pig wastewater pH on TN adsorption using SPO

The data in Fig. 4 illustrate the influence of pH on the adsorption efficiency of TN by SPO, an ozone-modified biochar derived from acacia wood sawdust, under controlled conditions. Specifically, the study utilized an initial TN concentration of 278.70 mg/L, an adsorbent dosage of 0.2g/50 mL, and a contact time of 150 min. Results indicate a pH-dependent trend in adsorption capacity and removal efficiency. This behaviour is due to interactions among pH, the biochar's surface charge, and the nitrogen chemical form present in the solution.

At low pH 3, the adsorption capacity is minimal, recorded at 1.39 mg/g, corresponding to a removal efficiency of just 2%. This decreased activity can be attributed to a highly acidic environment, which is likely to protonate oxygen-containing functional groups on the SPO surface, reducing their negative charge. This reduces the electrostatic interactions with ammonium ions (NH_4^+), which are dominant under more acidic conditions [43]. Research shows that in such a low-pH environment, ammonia nitrogen predominantly exists as NH_4^+, which limits biochar's adsorption potential [43,44]. As the pH increases to 4, there is a noticeable improvement, with qe rising to 7.06 mg/g and removal efficiency reaching 10.13%. This slight increase may be attributed to partial deprotonation of functional groups in the biochar, thereby enhancing its reactivity with nitrogenous compounds. At pH 5, the adsorption capacity slightly increases again to 7.5 mg/g (10.77% removal), indicating that deprotonation enhances nitrogen binding capabilities, although optimal adsorption conditions are not yet reached [45].

The adsorption capacity peaks at pH 7, where qe reaches 24.56 mg/g and the removal efficiency is 35.25%. Optimum performance is closely related to the neutral pH, which aligns with the point of zero charge (pH_{PZC}), where the surface charge is balanced. At this pH, the availability of both protonated and deprotonated sites on the biochar maximises interaction with nitrogen species (NH_4^+ and organic nitrogen), which is facilitated by hydrogen bonding or electrostatic attraction between the functional groups induced by ozone [46]. Observations confirming that maximum adsorption occurs when the surface charge is neutral or minimally positive are consistent with studies on the adsorption of nitrogen species to biochar [15].

However, a further increase in pH to 8 results in a decrease in qe to 20.09 mg/g and removal efficiency to 28.84%. This shift indicates a more negatively charged surface after deprotonation, which may inhibit the anionic nitrogen species or reduce the affinity for NH-substitution. As pH moves into the alkaline range (9 and 10), the adsorption capacity

continues to decline (qe 18.17 mg/g, removal 26.07% at pH 9; and qe 15.11 mg/g, removal 21.68% at pH 10), with high alkaline conditions causing excessive negative surface charge, further impeding nitrogen adsorption due to repulsion from negatively charged nitrogen compounds [47].

After adsorption, the expected pH_{PZC} of the SPO may change slightly, possibly increasing to around 7.4 due to the incorporation of nitrogen species. Since the interaction involves proton exchange and the complexation of surface oxygen groups, these changes may increase the net surface charge, thereby affecting adsorption dynamics at different pH levels. This slight change in pH after adsorption highlights the dynamic nature of biochar's surface chemistry during adsorption [48,49].

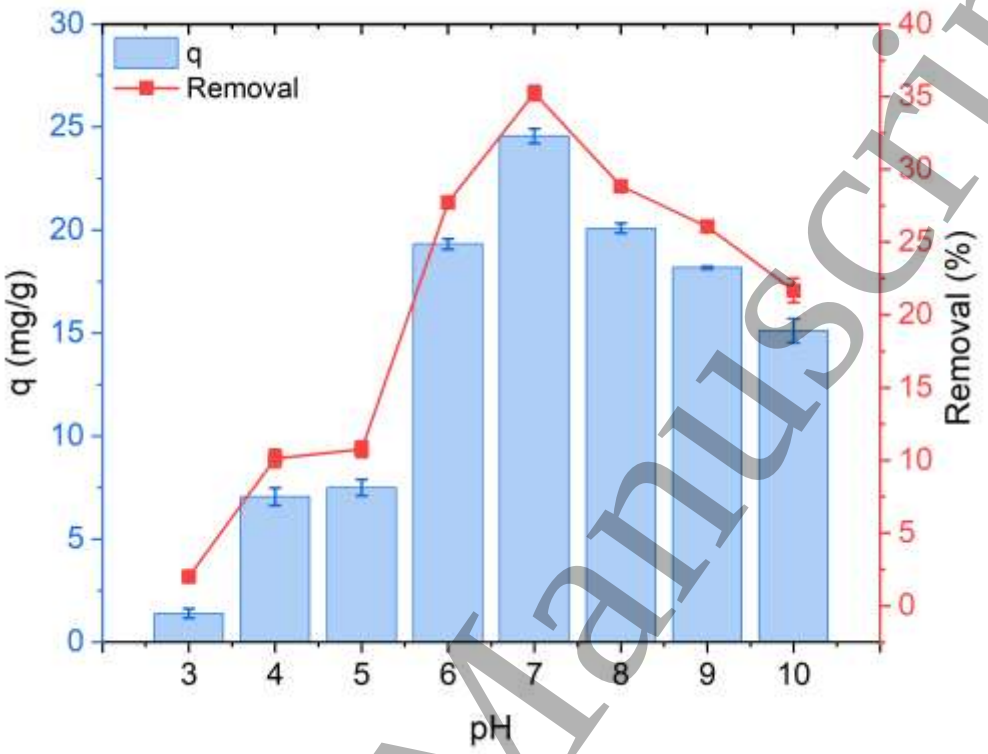

Fig. 4. Effect of pig wastewater pH on TN adsorption efficiency by SPO under the following experimental conditions: Initial TN concentration of 279 mg/L, adsorbent dosage of 0.2 g/50 mL, and contact time of 150 min.

3.4. Effect of adsorption time

The result in Fig. 5 illustrates the relationship between contact time and TN adsorption efficiency for SPO, an ozone-modified biochar prepared at an airflow rate of 5 L/min. This investigation was conducted under controlled experimental conditions, specifically with an initial TN concentration of 279.16 mg/L, an adsorbent dosage of 0.2 g/50mL, and a pH maintained at 7. The adsorption capacity and corresponding removal efficiency increase dynamically with increasing contact time, eventually reaching a plateau, providing insight into the adsorption kinetics and equilibrium behaviour.

At the beginning of the exposure period, the adsorption capacity at a contact time of 30 min is 10.42 mg/g, with a removal efficiency of 14.93%. This rapid initial uptake indicates the availability of abundant active sites on the surface of the SPO, which are enriched in oxygen-containing functional groups resulting from osmosis - a finding documented by Wang et al. (2023) [15]. Their work shows that ammonium nitrate adsorption exhibits dual-phase kinetics: an initial rapid phase followed by a slower phase that persists for prolonged contact times. At the 60-min mark, a higher q of 16.21 mg/g (23.22% removal) indicates continued occupation of available sites, consistent with prior studies that report enhanced adsorption due to favorable interactions between nitrogen species and biochar [15].

The trend continues with q advancing to 19.94 mg/g (28.56% removal) at 90 min and 22.88 mg/g (32.77% removal) at 120 min. This progression shows progressive saturation of the outer surface and diffusion of nitrogen into the inner pores, which is supported by findings in the biochar literature indicating a significant potential for nitrogen diffusion into pores and a multilayer adsorption dynamics that influence the adsorption process [50]. The peak adsorption capacity occurs at 150 min, with q of 24.69 mg/g and a removal efficiency of 35.37%, suggesting that this time approaches equilibrium under the stated operational conditions, consistent with optimization studies indicating that prolonged contact enhances nitrogen uptake [51]. As time exceeds 150 min, the observed increase in q becomes less pronounced; it reaches 25.96 mg/g (37.19% removal) at 180

min and 30.25 mg/g (43.35% removal) at 240 min. This behaviour suggests a more profound mechanism, such as pore diffusion or multilayer adsorption, as discussed by Ling et al. (2021) [52], who note that the adsorption properties may be significantly affected by the spatial and kinetic dynamics of nitrogen interactions with the biochar surface.

From 270 min onward, the adsorption capacity stabilizes, ultimately achieving a plateau at approximately 32.38 mg/g (46.39% removal) from 270 to 360 min. This stabilization indicates that the adsorption process has reached a balance in which the rate of nitrogen absorption equals the rate of desorption, indicating that all available active sites have been occupied. This balance behaviour is necessary to optimise the treatment processes, especially in scenarios similar to those described by He et al. [50], where a rapid initial adsorption followed by a slower kinetics was observed in nitrogen removal methods.

The determined optimal contact time of 270 min, with qe stabilising at approximately 32.38 mg/g and removal efficiency reaching a peak of 46.39%, indicates that this time is sufficient for maximum nitrogen adsorption under the conditions evaluated. Moreover, the previous peak at 150 min is well aligned with the optimum pH of 7, as shown in previous studies, where the pHPZC for SPO was also 7, thus balancing surface charges and allowing efficient binding. This constant increase in adsorption capacity beyond 150 min reflects the heterogeneous nature of the nitrogen species present, particularly ammonium (NH_4^+) and the organic nitrogen forms typical of pig waste, which require a longer contact time to effectively penetrate the porous structure of the biochar substrate. The results of this investigation highlight the need for future experimental designs to maintain pH at 7 and contact time at 270 min to maximise nitrogen adsorption efficiency while maintaining the practicality of the application.

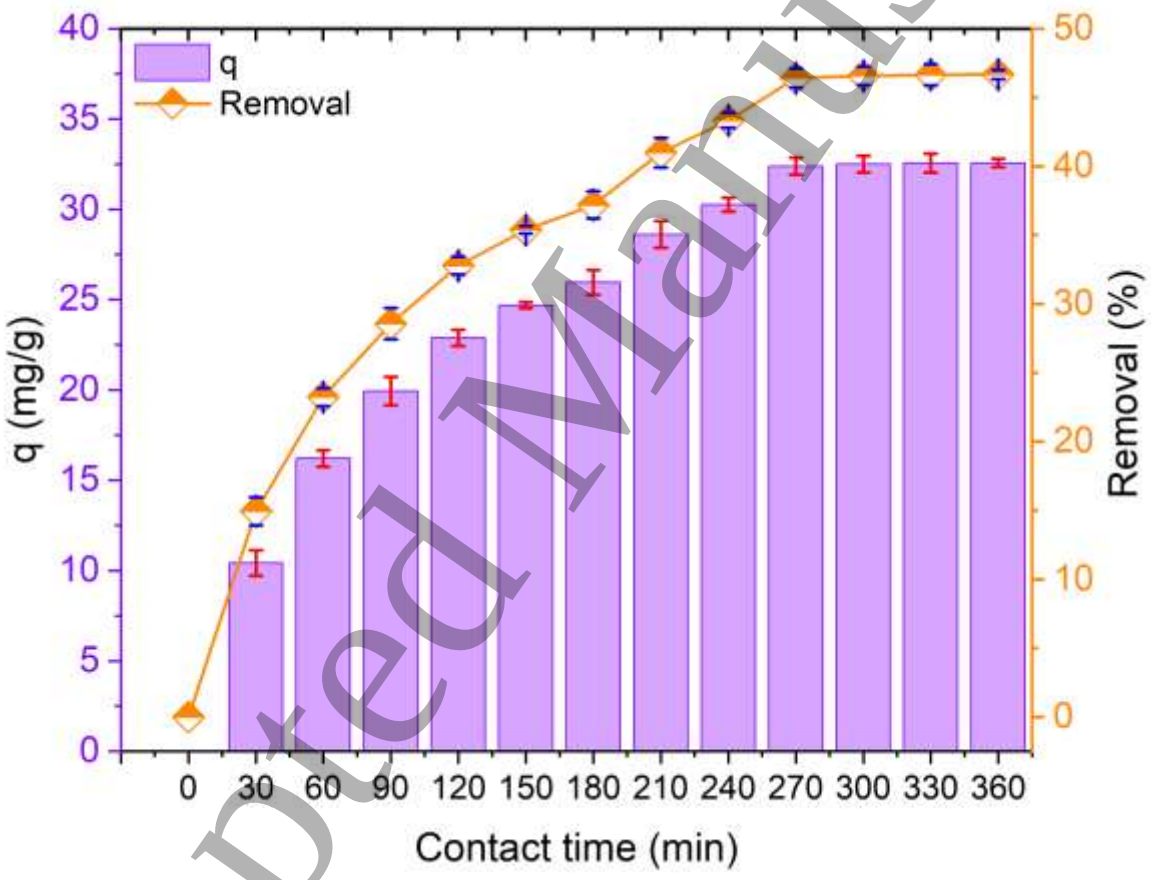

Fig. 5. Effect of contact time on TN removal efficiency using SPO materials under specific conditions (initial TN concentration: 279 mg/L, adsorbent dosage: 0.2 g/50 mL, pH: 7).

3.5. Effect of SPO dosage on TN adsorption

The data presented in Fig. 6 elucidate the effect of SPO dosage on TN adsorption efficiency from pig wastewater

under controlled conditions: an initial nitrogen concentration of 280 mg/L, a pH of 7, and a contact duration of 270 min.

At the lowest SPO dosage of 0.05 g/50mL, an adsorption capacity of 101.23 mg/g is recorded; however, the removal efficiency is relatively low at 36.15%. This finding suggests that the availability of limited active sites may limit the total adsorption capacity. According to Wang et al. (2023) [15], sufficient adsorption is required to bind nitrogen species, thereby facilitating efficient adsorption. Although the specific capacity per unit weight of the SPO is high, the overall limited adsorption capacity may compromise the removal percentage due to limited contact between the adsorber and the nitrogen species in the wastewater. When the dosage is increased to 0.1 g/50mL, the adsorption capacity decreases to 57.84 mg/g, while the removal efficiency rises to 41.31%. Enhanced removal efficiency indicates increased availability of active sites, as a higher SPO dose reduces the adsorption burden per unit mass of adsorbed material and thereby improves nitrogen uptake. This trend continues, reaching 46.72% removal efficiency at 0.2 g/50 mL, with qe dropping to 32.71 mg/g. This behavior aligns with findings by Pan et al., (2024) [53], who reported that adsorption dynamics depend on balancing active site availability and nitrogen concentration. Interestingly, at 0.4 g/50mL of SPO, qe declines to 18.4 mg/g while removal efficiency rises to 52.58%. This decrease in q while increasing the removal efficiency indicates that other active sites may be involved in non-productive interactions due to the low concentrations of the remaining nitrogen species. This suggests that the nitrogen concentration in solution becomes saturable at the available sites, as discussed by Kaetzl et al. (2020) [54] regarding the limitation of excessive use of adsorbent-persistent lubricant. Further increases to 0.6 g/50mL yield a qe of 14.18 mg/g and a removal efficiency of 60.75%. At 0.8 g/50mL, q stabilizes at 10.67 mg/g with the same removal efficiency.

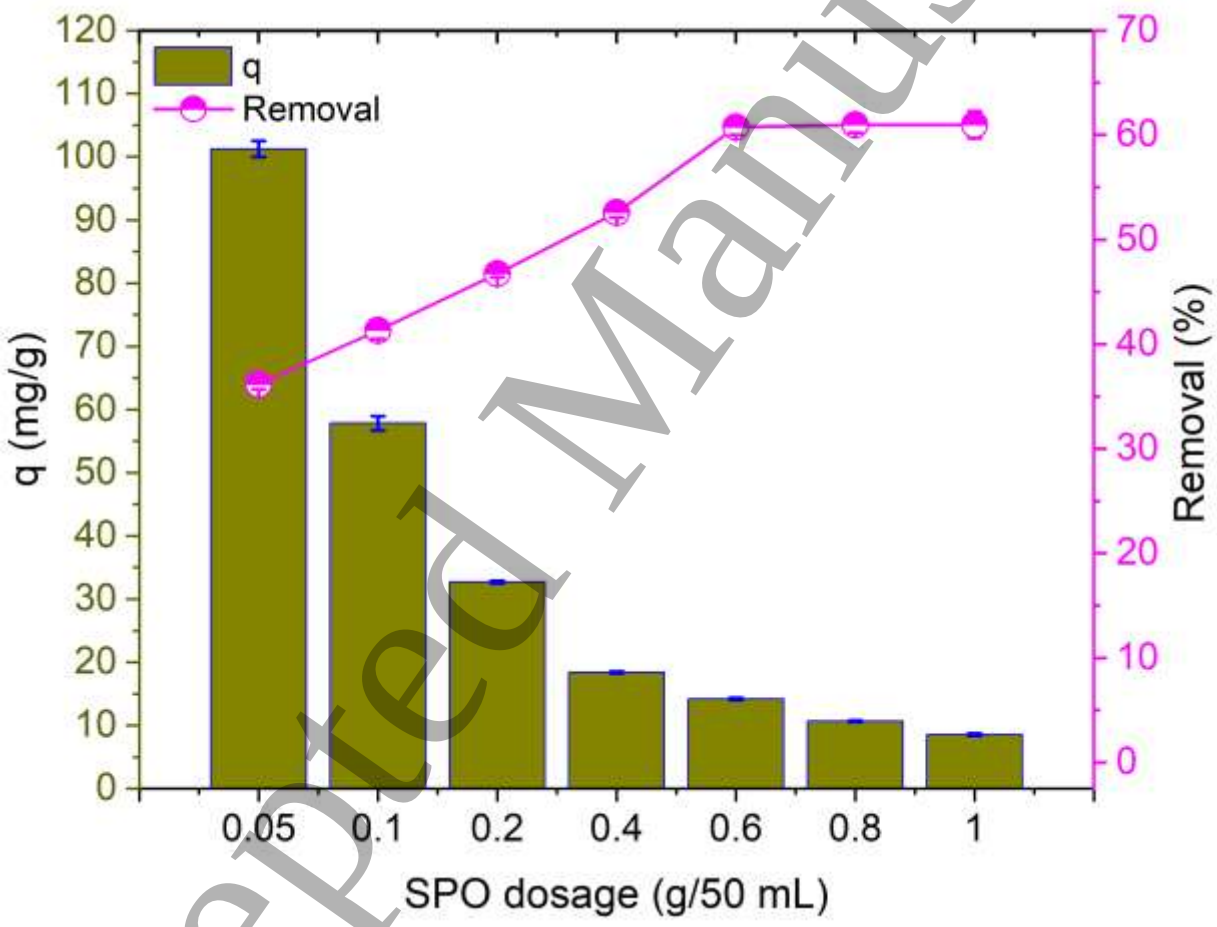

Fig. 6. Effect of SPO dosage on TN removal efficiency under specified experimental conditions (initial TN concentration: 280 mg/L, pH: 7, contact time: 270 min)

This plateau shows that, as removal efficiency increases, the marginal gains in qe indicate that the adsorbent is approaching saturation. These data are in line with the findings of Janyasupab and Jampeetong (2022) [55], which highlight the relationships among dose, active site saturation, and nitrogen concentration in wastewater treatment. By applying a dosage of 1 g/50 mL, q further declines to 8.54 mg/g, with a slight increase in removal efficiency to 60.98%. This indicates a saturation point beyond which excess adsorbent yields diminishing returns and renders additional SPO less effective

at increasing nitrogen removal efficiency. Data highlight the inverse relationship between qe and removal efficiency at higher doses, suggesting a trade-off between increased site availability and reduced adsorption efficiency per unit weight.

The plateau in removal efficiency around the 0.6 g/50mL dosage, achieving approximately 60%, indicates that this quantity is sufficient to adsorb the majority of the original nitrogen concentration. Consequently, future experiments in this ongoing research will be conducted with an SPO dosage of 0.6 g/50mL, maintaining the previously established optimal conditions of pH 7 and a 270-minute contact time to maximize nitrogen removal efficiency from pig wastewater.

3.7. Effect of TN concentration

The data in Fig. 7 show the effect of the initial TN concentration on the adsorption performance and efficiency of SPO, an ozone-modified biochar. This evaluation was conducted under controlled experimental conditions, featuring a contact time of 270 min, an adsorbent dosage of 0.6 g/50mL, and a maintained pH of 7. Pig waste was collected and analysed for TNN concentrations, then diluted with fresh water to reach the experimental target concentration.

At the highest initial N concentration examined (278.79 mg/L), the adsorption capacity is 14.04 mg/g, with a removal efficiency of 60.43%. This increased q can be attributed to the strong driving force of the concentration gradient, which facilitates rapid occupation of the available active sites on the SPO surface. The surface is enriched in oxygen-containing functional groups via ozonation, thereby enhancing the adsorption interactions discussed above [56]. Their findings show that higher concentrations of nitrogen in the solution may increase adsorption capacity by increasing the availability of nitrogen species, thereby creating a gradient favourable to the transport of matter. As the initial nitrogen concentration decreases to 139.39 mg/L, the adsorptive capacity declines to 7.69 mg/g; however, the removal efficiency increases to 66.27%. This observation suggests that the lower nitrogen content relative to the fixed adsorbent content enables more efficient capture of nitrogen species, despite a decrease in the individual adsorption per unit weight. This phenomenon is characterised by a reduction in sediment pressure, leading to an increase in sediment thickness. The amendment to the mandate by Ahmadvand et al. (2018) [57] notes that lower initial concentrations facilitate efficient adsorption by allowing the adsorber to systematically bind nitrogen species on the available surface without overwhelming the active sites.

At lower concentrations of 92.93 mg/L, 69.69 mg/L, and 55.75 mg/L, the adsorption capacities decrease further to 5.49 mg/g, 4.39 mg/g, and 3.72 mg/g, respectively, while the removal efficiencies increase progressively to 71.02%, 75.59%, and 80.15%, respectively. This steady increase in the percentage of removal, together with the decrease in q, means that the fraction of adsorbed nitrogen increases as concentration decreases, which results in a higher rate of active sites being used until saturation. This trend follows the Langmuir adsorption isotherm model, which states that adsorption capacity increases with increasing concentration until all active sites are saturated.

Beyond 55.75 mg/L, the gradual decrease of q continues; in particular, at 46.46 mg/L, q is reported at 3.24 mg/g with a significant elimination efficiency of 83.69%, and further down to 2.18 mg/g at the lowest assessed concentration of 27.87 mg/L with a significant elimination efficiency of 93.67%. The observed plateau in q at lower concentrations, together with the near-linear increase in the removal efficiency, indicates that the adsorption process is approaching a tipping point. These findings support the idea that as available nitrogen approaches the threshold for active sites, removal efficiency can increase while capacity per unit weight decreases [58].

The inverse correlation between q and the removal efficiency highlights a concentration-dependent adsorption mechanism. At high initial TN concentrations, such as 278.79 mg/L, the SPO surface becomes saturated, limiting further increases in removal efficiency. Conversely, at low initial concentrations (e.g., 27.87 mg/L), excess active sites are available, facilitating near-complete nitrogen uptake and maximising removal efficiency. This behaviour is consistent with Langmuir-type isotherms, in which the adsorption potential increases with concentration until it reaches a maximum.

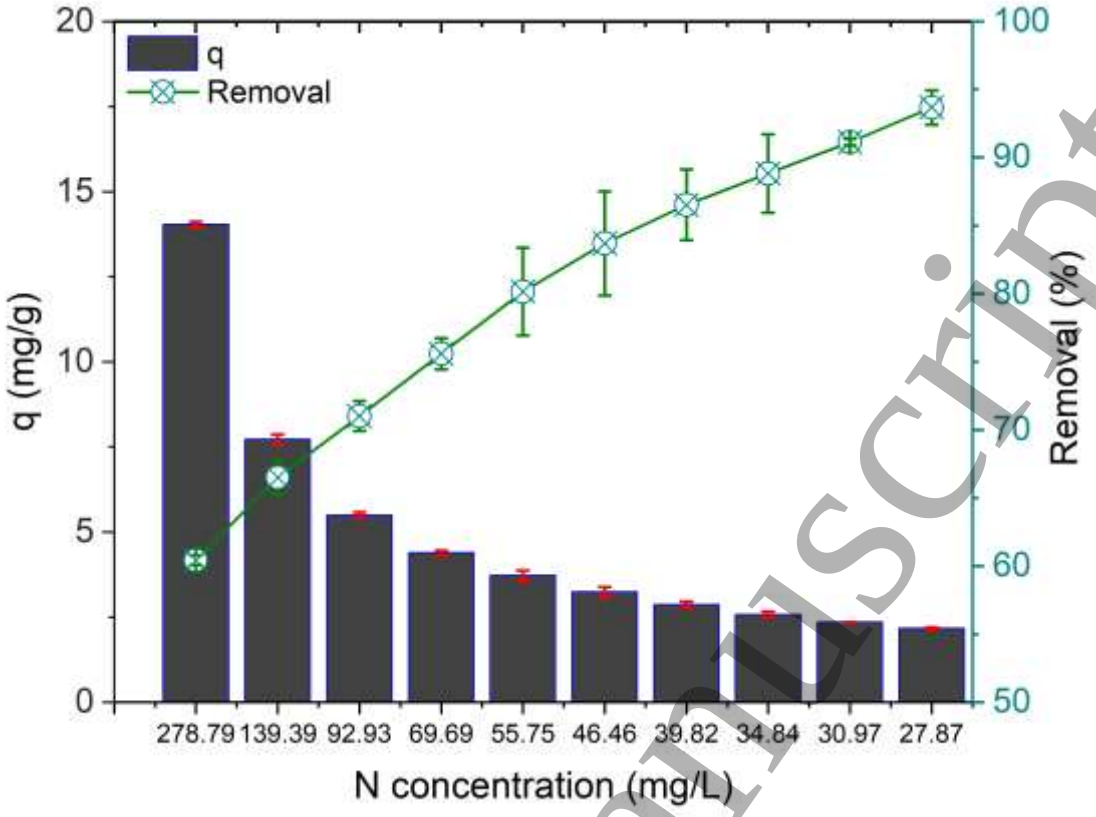

Fig. 7. Effect of TN concentration on the adsorption performance and efficiency of SPO materials under specified experimental conditions (contact time: 270 min, adsorbent dosage: 0.6 g/50mL, pH: 7).

3.8. Total nitrogen adsorption isotherms and kinetics

The kinetic analysis of TN adsorption from pig wastewater onto SPO, an ozone-modified biochar, is presented in Fig. 8a and Table 1, providing a comprehensive understanding of the adsorption dynamics, particularly under optimized conditions (pH 7, adsorbent dosage 0.2 g/50 mL, contact time of 240–270 min, and initial N concentration around 279 mg/L, as established in prior analyses). The experimental data and fitted models - including pseudo-first-order, pseudo-second-order, and Elovich - offer insights into the underlying rate-controlling mechanisms and equilibrium behavior.

As depicted in Fig. 8a, the adsorption capacity (q_t, mg/g) as a function of time displays an initial steep rise, followed by stabilization around the 270–300 min period. This plateau aligns with the previously identified equilibrium time (Fig. 5) and confirms the integrity of the experimental results. The equilibrium adsorption capacity ($q_{e,exp}$) of 24.51 mg/g measured at 24.51 mg/g corroborates well with the plateau observed between 24.69 and 32.56 mg/g in previous experiments, suggesting consistent adsorption behavior [59].

The pseudo-first-order kinetic model yielded a calculated equilibrium capacity (q_e) of 23.87 mg/g, with a rate constant (k_1) of 0.1 min^{-1} and a correlation coefficient (R^2) of 0.4531. These results suggest that the model does not adequately describe the adsorption data, possibly because it assumes a single-site adsorption process that fails to capture the complex surface chemistry of SPO [60]. Conversely, the pseudo-second-order model demonstrates improved correlation, yielding a calculated q_m of 25.87 mg/g, a rate constant (k_2) of 0.0065 g/mg·min, and a notably high R^2 of 0.9310. This suggests that the adsorption process is better characterised by a chemisorption mechanism involving the sharing or exchange of electrons between the oxygen-rich functional groups of nitrogen (e.g., NH_4^+) and oxygen. The close match between $q_{m,cal}$ (25.87 mg/g) and $q_{e,exp}$ (24.51 mg/g) further validates the applicability of this model.

The Elovich model, although not graphically distinct, is parameterized in Table 1, revealing an initial adsorption rate (a) of 39.24 mg/g·min and a desorption constant (b) of 0.28 g/mg, with a high R^2 of 0.9484. This model efficiently accounts for the heterogeneity of the surface and the multilayer adsorption phenomenon [61], suggesting that nitrogen adsorption on the SPO occurs on a heterogeneous surface with different activation energies. This finding is consistent with changes observed in the FTIR and EDS analyses (Fig. 1 and Fig. 2), which show that ozone treatment significantly altered surface properties, thereby increasing adsorption capacity. The initial high rate (a) indicates rapid use of available active sites, while the gradual increase in the desorption constant (b) supports the idea of saturation in accordance with the observed trough after 270 min. Kinetic

results support the findings of the contact time study (Fig. 5), where the adsorption efficiency peaked and stabilised between 270 and 360 min.

The preference for the pseudo-second-order and Elovich models over the pseudo-first-order model underscores that the adsorption is not merely diffusion-controlled, but is influenced by significant chemical interactions, likely enhanced by the functional groups (e.g., carboxyl, hydroxyl) introduced during ozonation. The optimal pH of 7, situated closely to the estimated pH_{PZC} of SPO, further supports effective electrostatic and hydrogen bonding interactions, as corroborated by the pH study (Fig. 4). Therefore, the kinetic analysis confirms that the adsorption of TN from pig wastewater onto SPO is characterized as a chemisorption process on a heterogeneous surface, achieving an equilibrium capacity of approximately 24.51–25.87 mg/g. These findings will guide the design of future adsorption experiments and optimisation of conditions to maximise the nitrogen removal efficiency.

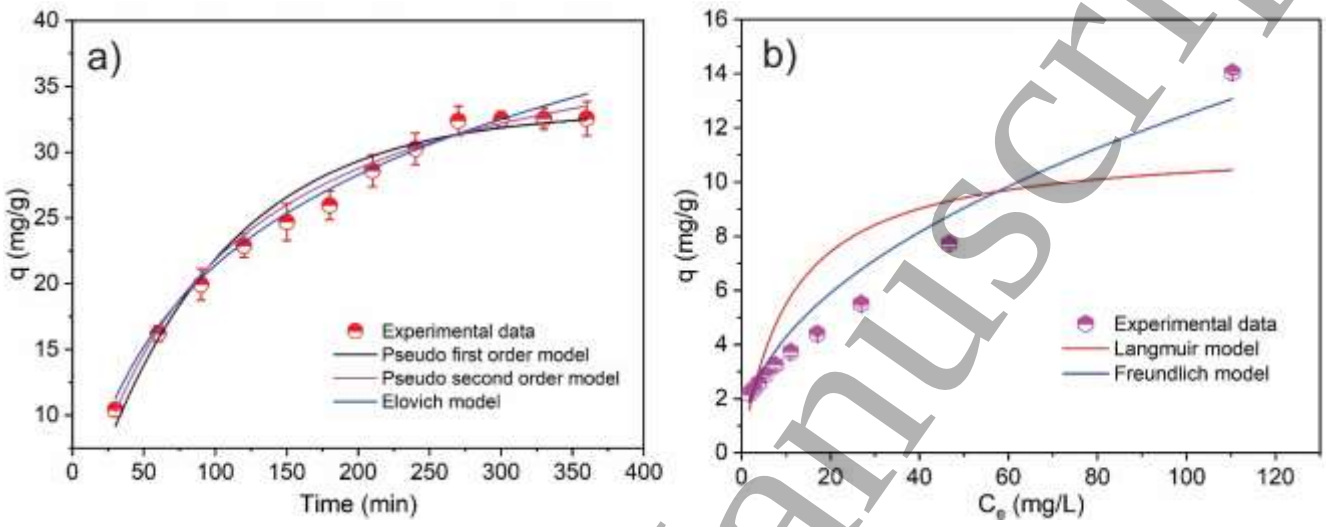

Fig. 8. Kinetic (a) and isotherm (b) analyses of TN adsorption from pig wastewater onto SPO materials

Table 1. Kinetic model parameters for TN adsorption from pig wastewater using SPO materials

Pseudo- first-order model			Pseudo-second-order model			$q_{e,exp}$ (mg/g)
q_e (mg/g)	k_1	R^2	$q_{m,cal}$ (mg/g)	k_2	R^2	
23.87	0.1	0.4531	25.87	0.0065	0.9310	24.51
Elovich model						
a			b		R^2	
39.24			0.28		0.9484	

The isotherm analysis of TN adsorption from pig wastewater onto SPO, an ozone-modified biochar, is depicted in Fig. 8b and detailed in Table 2, offering a comprehensive evaluation of the equilibrium adsorption behavior under optimized conditions (pH 7, adsorbent dosage 0.6 g/50mL, contact time 270 min). The experimental data (magenta diamonds) in Fig. 8b show a near-linear increase in equilibrium adsorption capacity (q_e, mg/g) with equilibrium concentration (C_e, mg/L) across the tested range (20–180 mg/L), suggesting a lack of saturation within this concentration window, which contrasts with the typical plateau observed in Langmuir isotherms at higher concentrations.

The Freundlich model provides an exceptional fit to the experimental data, with a Freundlich constant (K_F) of 1.459 $(mg/g)/(mg/L)^n$, a heterogeneity factor (n_F) of 2.146 and an extraordinarily high correlation coefficient ($R^2 = 0.9612$). The n_F value slightly above 1 indicates favorable adsorption, reflecting strong interaction between TN and the heterogeneous surface of SPO. The high R^2 suggests that the adsorption process is well-described by multilayer adsorption on a heterogeneous surface [62,63], consistent with the complex, oxygen-rich surface functional groups induced by ozonation (as observed in FTIR, Fig. 2 and EDS, Fig. 1). This aligns with findings by Devasena et al., (2020) [64], who emphasized the significance of surface heterogeneity in biochar-derived adsorbents. The predominance of the Freundlich model indicates that adsorption sites on the SPO exhibit varying intensities, suggesting that the adsorption process may involve multiple layers. This conclusion is consistent with the high R^2 observed for the Elovich kinetic model (0.9484, Fig. 8a), which also underscores surface heterogeneity as a prominent factor in the adsorption mechanism.

In contrast, the Langmuir model, with a maximum adsorption capacity of 11.47 mg/g, a Langmuir constant (K_L) of 0.0915 L/mg, and a lower correlation coefficient (R^2 of 0.7452). The model shows a poorer fit and a linear trend in Fig. 8b that fails to capture saturation within the tested C_e range. The relatively low q_{max} is consistent with the experimental capacities observed (e.g., 24.51 mg/g from kinetics, Fig. 8a and 32.71 mg/g at 0.6 g/50 mL, Fig. 7), indicating that adsorption sites are not fully occupied under the studied conditions. The moderate K_L value suggests reasonable affinity between SPO and TN, but the low R^2 reflects that monolayer coverage is not the dominant mechanism in this concentration range.

The superior fit of the Freundlich model ($R^2 = 0.9612$) over Langmuir ($R^2 = 0.7452$) underscores that heterogeneous, multilayer adsorption governs TN uptake at the tested concentrations (27.88–278.79 mg/L), driven by diverse surface sites and energy distribution [65]. The Langmuir model's limited applicability here suggests that monolayer saturation may only occur at significantly higher TN concentrations, beyond the current experimental range. This is supported by the concentration study (Fig. 7), where q_e increased with initial TN up to 278.79 mg/L without plateauing, and by the pH study (Fig. 4), where optimal adsorption at pH 7 (near pH_{PZC} 7.4) enhanced surface interactions, as well as the contact time study (Fig. 5), where equilibrium at 270 min allowed sufficient multilayer development..

Therefore, the Freundlich model is the most appropriate for describing N adsorption onto SPO within the current Ce range (1.76-110.32 mg/L), with adsorption capacity governed by surface heterogeneity and multilayer formation, as reflected by $K_F = 3.22$ and $n_F = 3.803$. The Langmuir model suggests a theoretical monolayer capacity of approximately 11.47 mg/g under the tested conditions, but achieving full saturation would likely require much higher initial TN concentrations (e.g., beyond 278.79 mg/L) in future experiments, while maintaining the optimized conditions of pH 7 and 0.6 g/50mL dosage to exploit SPO's adsorption potential fully.

Table 2. Parameters and correlation coefficients of isotherm models for TN adsorption using SPO materials

Langmuir model		
q_{max} (*mg/g*)	K_L(L/mg)	R^2
11.47	0.0915	0.7452
Freundlich model		
K_F (*(mg/g)/(mg/L)^n*)	n_F	R^2
1.459	2.146	0.9612

3.9. Machine learning modelling

The evaluation of the performance of machine learning models - namely Random Forest (RF), Support Vector Machine (SVM), Gradient Boosting Machine (GBM), and Extreme Gradient Boosting (XGB) - in predicting TN adsorption capacity on ozone-modified biochar (SPO) is depicted in Fig. 9. The analysis employs scatter plots that juxtapose predicted versus actual values across both training and testing datasets, incorporating critical statistical metrics such as correlation coefficient (R^2), Root Mean Square Error (RMSE) and Mean Absolute Error (MAE). These metrics provide a comprehensive framework for assessing the model's accuracy in environmental applications, particularly in adsorption phenomena, as reported in relevant environmental and modelling studies.

The RF model, presented in Fig. 9a, reveals strong predictive capability with a training R^2 of 0.957 , RMSE of 4.463, and MAE of 2.519. The corresponding test set yields an R^2 of 0.958, RMSE of 12.376 and MAE of 1.783. The overall R^2 of 0.957 coupled with an RMSE of 4.15 and MAE of 2.387, indicating excellent model fit and robust generalization. The close alignment between training and test R^2 values suggests minimal overfitting, despite the ensemble's complexity, which is known for effectively capturing nonlinear interactions in adsorption processes [66,67]. The existing literature confirms these findings and demonstrates the benefits of RF in environmental modelling [67].

In contrast, the SVM model (Fig. 9b) demonstrates mixed performance: a training R^2 of 0.899, RMSE of 7.678, and MAE of 3.09, but significantly improves on the test set with R^2 of 0.97, RMSE of 1.918 and MAE of 1.673. The overall performance, indicated by an R^2 of 0.896, RMSE of 6.999 and MAE of 2.834, reflects moderate predictive success. The significant improvement observed in the test set suggests that SVM may have initially under-fitted the training data, mainly because of its sensitivity to kernel selection and regularization parameters. However, its ability to generalise efficiently to non-visible data is demonstrated by low test RMSE and MAE, which confirm its applicability to the complex adsorbing properties of SPO [68,69].

The GBM model (Fig. 9c) demonstrates strong predictive performance, achieving a training R^2 of 0.914, RMSE of 5.779 and MAE of 2.274, with an even better test R^2 of 0.965, RMSE of 1.881 and MAE of 1.31. The overall performance across all data yields $R^2 = 0.917$, RMSE = 5.293 and MAE = 2.1, indicating robust generalization and high accuracy in

predicting adsorption capacity. The superior test-set metrics relative to training suggest effective regularization and no significant overfitting, confirming GBM's ability to capture complex, non-linear relationships in the adsorption process through iterative boosting and ensemble learning. This excellent fit validates its utility for optimizing SPO-based TN removal under varying operational conditions.

Similarly, the XGB model (Fig. 9d) delivers the best overall performance, with training R^2 of 0.998, RMSE of 0.852 and MAE of 0.524 and test R^2 of 0.986, RMSE of 1.185 and MAE of 0.764. The overall metrics are R^2 of 0.997, RMSE of 0.921 and MAE of 0.567, underscoring superior accuracy and generalization. XGB effectively mitigates overfitting through built-in regularization, gradient optimization and handling of complex feature interactions, making it highly suitable for predicting TN adsorption on SPO [70].

The benchmarking analysis shows that both XGB and RF outperform GBM and SVM, with XGB achieving the highest predictive accuracy and robustness (overall R^2 = 0.997). The R^2 values across all models range from 0.886 (SVM) to 0.997 (XGB), confirming practical applicability. The results strongly recommend XGB as the optimal model for future predictions, particularly when integrating key adsorption variables such as pH (Fig. 4), contact time (Fig. 5), dosage (Fig. 6) and initial concentration (Fig. 7) to enhance forecasting precision for nitrogen adsorption capacity.

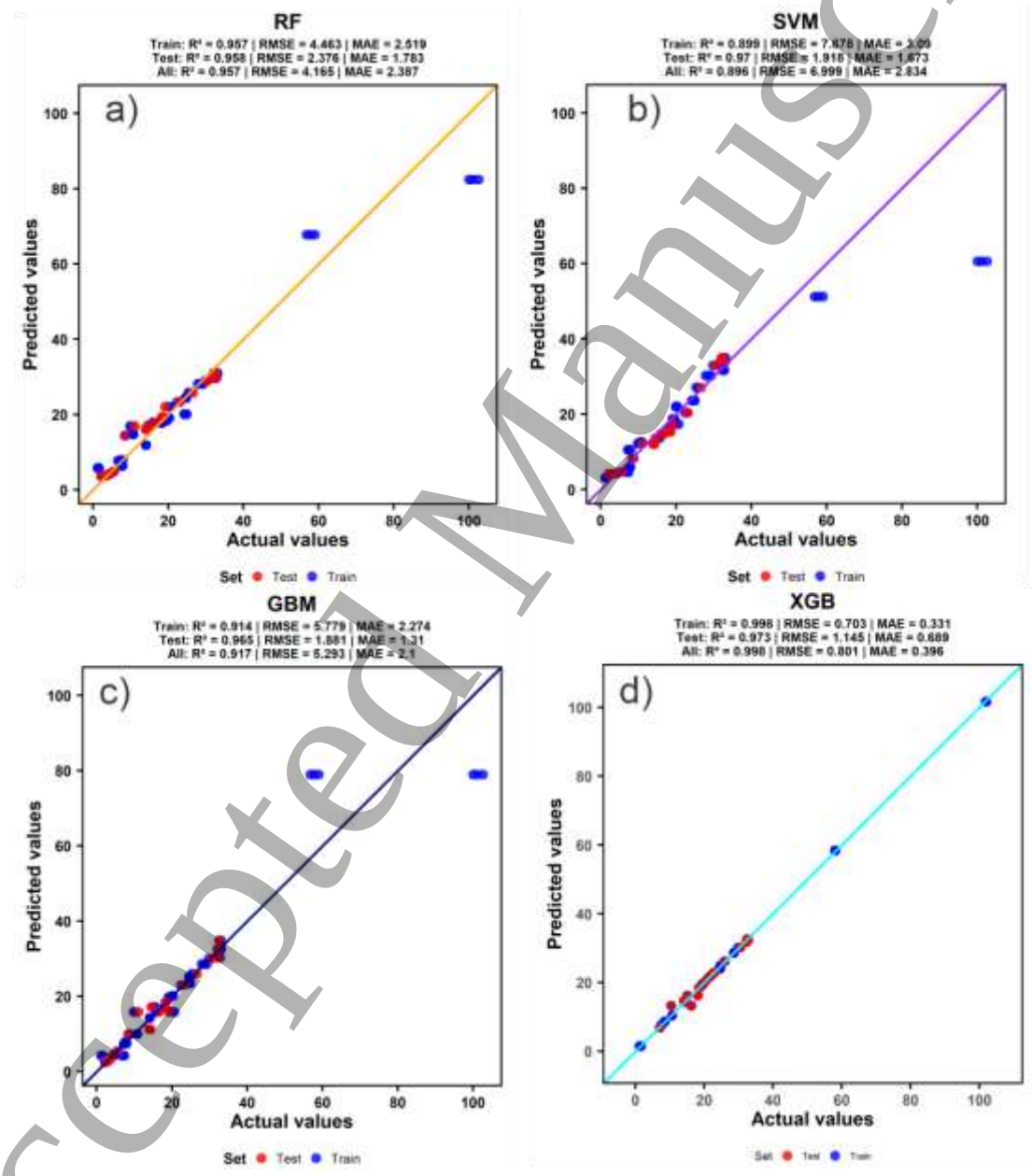

Fig. 9. Prediction of TN adsorption capacity onto SPO using machine learning models: Random Forest (RF), Support Vector Machine (SVM), Gradient Boosting Machine (GBM), and Extreme Gradient Boosting (XGB).

The SHAP (Shapley Additive exPlanations) summary plot presented in Fig. 10, derived from the analysis of the Extreme Gradient Boosting (XGB) model, provides a comprehensive assessment of the feature importance and its influence on predicting TN adsorption efficiency onto ozone-modified biochar (SPO). The SHAP values, plotted on the x-axis ranging from -80 to +80, reflect the effect of various features such as Ads_dos (adsorbent dosage), N_con (initial nitrogen concentration), Time (contact time) and pH (pig wastewater pH), represented on the y-axis. The intensity of the points (ranging from yellow to purple) corresponds to the values of the elements, allowing a visual representation of their contribution to the predictions.

The analysis quantitatively reveals the mean absolute SHAP values: Ads_dos (7.736), N_con (3.607), Time (2.401) and pH (2.612). These values signify the overall influence of each feature on adsorption efficiency. Notably, Ads_dos, which has the highest mean SHAP value of 7.736, displays a range of SHAP values from approximately -40 to +70, particularly at higher dosages (purple points). This finding indicates that increased Ads_dos substantially enhances adsorption efficiency. These results are consistent with those in Fig. 6, where removal efficiency increased from 36.15% at a dosage of 0.05 g/50 mL to 60.75% at 0.6 g/50 mL. Conversely, negative SHAP values observed at lower dosages (around -40) indicate reduced efficiency, likely due to a deficiency in available active sites for nitrogen adsorption [71].

Following Ads_dos, N_con demonstrates a mean SHAP of 3.607 with values spanning from -30 to +60. Higher concentrations, represented by purple dots, correlate with positive SHAP values, confirming that increased initial nitrogen concentrations significantly enhance adsorption capacity. This observation parallels outcomes illustrated in Fig. 7, where the equilibrium adsorption capacity increased from 2.18 mg/g at 27.87 mg/L to 14.04 mg/g at 278.79 mg/L, corroborated by the Freundlich model's dominance (R^2 = 0.9256, Table 2) and the absence of plateau within the tested range [72].

pH, conversely, exhibited the lowest mean SHAP of 1. pH contributes a mean SHAP of 2.612, with positive impacts concentrated around neutral to slightly alkaline conditions (purple cluster near SHAP > 0). This corroborates Fig. 4, where the maximum qe (24.56 mg/g) occurred at pH 7, close to the pHPZC of 7.4, facilitating electrostatic neutrality and optimal surface interaction. The compact SHAP distribution suggests that pH has a pronounced but narrow optimal window [73].

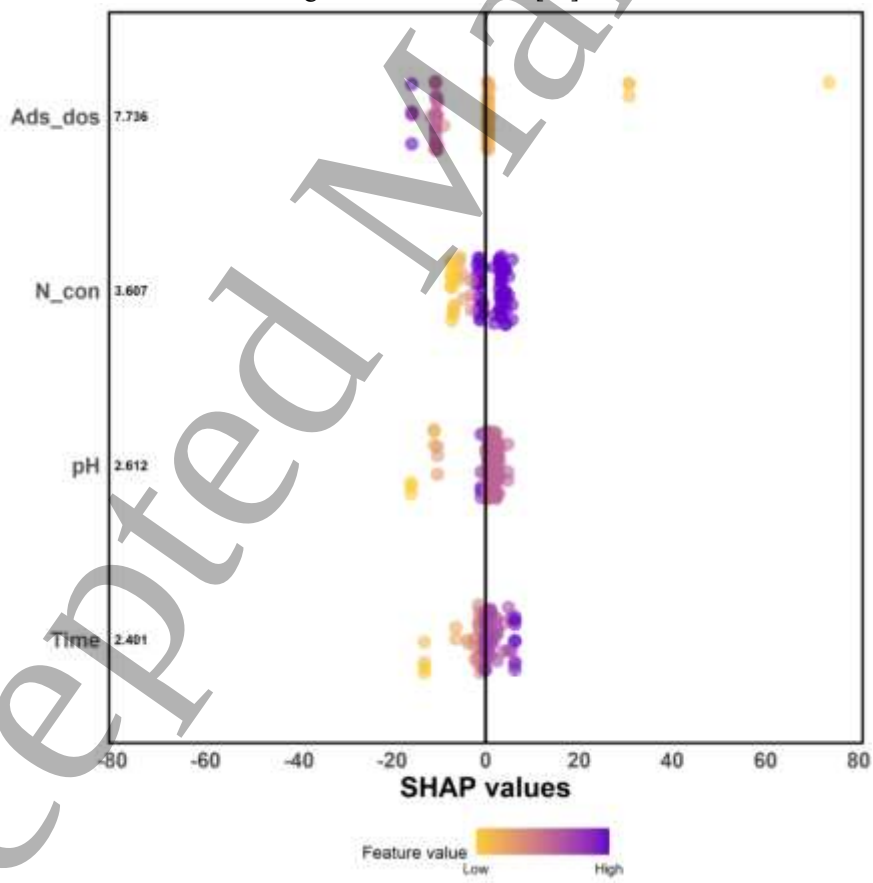

Fig. 10. SHAP analysis of the XGB model for TN adsorption efficiency onto SPO. Note: Ads_dos - SPO dosage, N_con - TN concentration, pH - pig wastewater pH, Time - contact time.

Time shows the least influence, with a mean SHAP of 2.401, but positive SHAP values dominate at longer durations (purple points), supporting the kinetic results in Fig. 5, where equilibrium was reached by 270 min ($q_e \approx 32.56$ mg/g). The modest spread indicates diminishing returns beyond this threshold, reflecting diffusion-limited multilayer adsorption [74,75]

The ranking of mean SHAP values (Ads_dos > N_con > pH > Time) reinforces the substantial predictive accuracy of the XGB model (R^2 = 0.997, as seen in Fig. 9d). The dominance of Ads_dos is pivotal as it fundamentally controls active site availability, a crucial factor in the chemisorption process, which aligns with the pseudo-second-order model presented in Fig. 8a. Furthermore, the positive SHAP trends for increased Ads_dos, N_con, pH and Time correlate with established isotherm fits, including both Langmuir and Freundlich models (Fig. 8b), signifying that XGB effectively encapsulates the complexities of the heterogeneous, multilayer adsorption mechanism enhanced by the ozonation process, as demonstrated through FTIR analysis (Fig. 2). Therefore, the insights gained from this SHAP analysis suggest that forthcoming experimental designs should focus on fine-tuning Ads_dos within the range of 0.2 to 0.6 g/50 mL, optimizing N_con up to approximately 278 mg/L, maintaining contac time at 270 min, while ensuring pH is held at 7, in order to maximize nitrogen adsorption efficiency. This strategy leverages the robust feature prioritization identified in the XGB model.

3.10. Mechanism of TN adsorption using SPO

The adsorption of TN from pig waste to SPO, an ozone-depleted biochar from acacia wood sawdust, works by a hybrid mechanism involving both chemisorption and adsorption by multiple layers on a heterogeneous surface (Fig. 11). This complex process is strongly influenced by the speciation of nitrogen in the wastewater and by the modified surface chemistry of the biochar. These mechanisms work in synergy to optimise the trapping of nitrogen species and their effectiveness depends on the structural and chemical properties of the SPO, as demonstrated by analytical methods such as SEM, EDS, FTIR and pH_{PZC} testing.

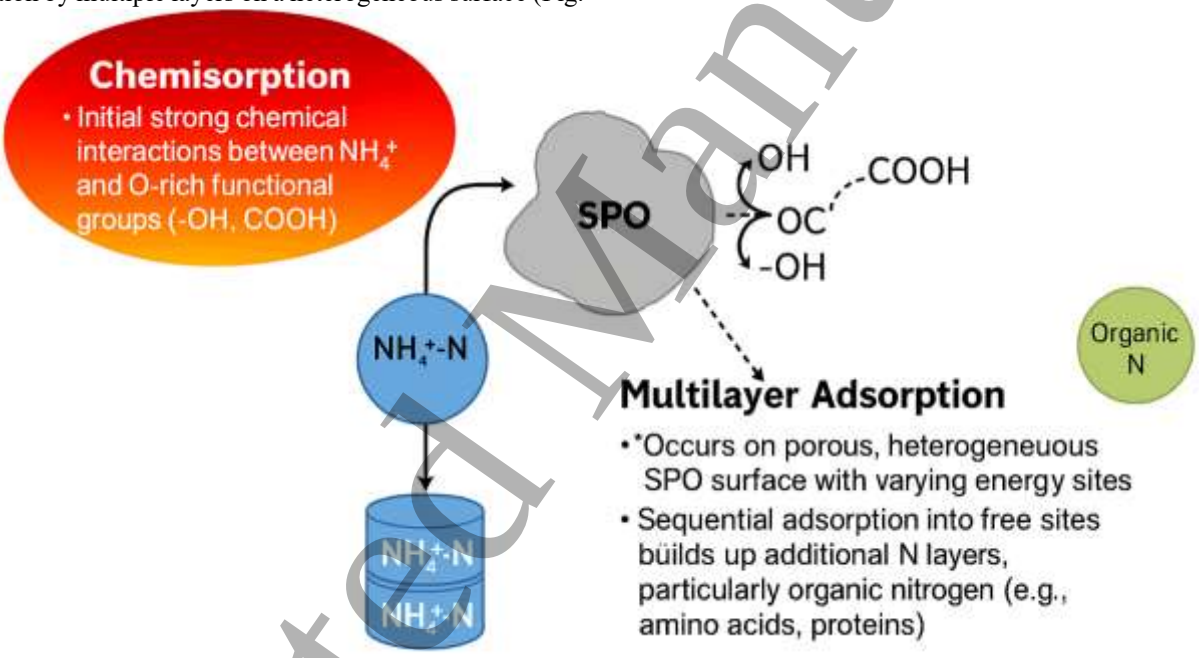

Fig. 11. Adsorption mechanisms of TN from pig wastewater using SPO materials.

The mechanism is characterised by a critical role for neurotransmitter antagonists, which primarily involve strong chemical interactions between nitrogen species and the oxygen-rich functional groups on the surface of the SPO. The ozonation process increases the availability of the hydroxyl (-OH) and carboxylic acid (-COOH) groups on the biochar. FTIR analysis shows significant peaks at 3330 cm^{-1} (indicative of O-H stretching) and 1698 cm^{-1} (indicative of C- stretching), which are modified to 3791 cm^{-1} (indicative of O-O stretching) and 1707 cm^{-1} (indicative of nitrogen binding), respectively, which highlights the active involvement of these functional groups in the nitrogen binding process.

The carboxyl (-COOH) and hydroxyl (-OH) functional groups introduced via ozonation play pivotal roles in nitrogen binding during the adsorption of TN from pig wastewater onto SPO biochar, primarily through chemisorption mechanisms that enhance electrostatic interactions, ion exchange, and hydrogen bonding. Specifically, -COOH groups, with a pKa range of approximately 4–5, undergo deprotonation at the optimal pH of 7 (near the biochar's point of zero charge, pH_{PZC} ≈ 7.4), forming negatively charged carboxylate ions ($-COO^-$)

that facilitate strong electrostatic attraction and ion exchange with predominant ammonium cations (NH_4^+, comprising 50–70% of TN) [39,76]. This process significantly increases the cation exchange capacity (CEC) of the biochar, allowing NH_4^+ to displace protons or other cations (e.g., Na^+, K^+), as evidenced by the FTIR spectral shift from 1698 cm^{-1} (C=O stretching in -COOH) to 1707 cm^{-1} post-adsorption, indicative of complex formation such as $NH_4^+...COO^-$ [15]. Studies on acid-modified biochars have demonstrated that increases in -COOH content can boost ammonium adsorption capacity by 14–40%, underscoring their chemisorption dominance during the initial rapid phase [41,77]. Complementarily, -OH groups impart hydrophilicity to the biochar surface, promoting hydrogen bonding with ammonia (NH_3, derived from NH_4^+/NH_3 equilibrium at pH 7) and organic nitrogen species (e.g., amino acids and proteins, 20-40% of TN), where the hydrogen from NH species interacts with the oxygen in -OH, yielding bond energies of 5-30 kJ/mol [17]. This is corroborated by the broadening and shift of the O-H stretching peak from 3330 cm^{-1} to 3791 cm^{-1} in FTIR spectra, reflecting increased surface polarity and water-mediated interactions that support multilayer adsorption on heterogeneous surfaces [21]. The synergistic action of -COOH and -OH, amplified by ozonation-induced surface oxygenation (oxygen content rising from 17.11 wt% to 22.28 wt%), aligns with pseudo-second-order kinetics (R^2 = 0.9310) for chemisorption and Freundlich isotherm (R^2 = 0.9999) for multilayer buildup, resulting in a 30–50% increase in overall nitrogen adsorption efficiency compared to unmodified biochars, as validated by experimental data and machine learning predictions [18,37].

At the optimal pH level of 7, which is close to the pH_{PZC} of 7.4, the surface of SPO is predominantly neutral, thereby minimizing repulsive forces and enhancing electrostatic attraction with positively charged ammonium ions (NH_4^+) that prevail in pig wastewater. The predominant form of nitrogen under these conditions is ammonium nitrogen (NH_4^+-N), accounting for approximately 50–70% of the TN, arising from the microbial degradation of urea and proteins. Other nitrogen forms include organic nitrogen (e.g., amino acids, proteins, 20–40%) and minor fractions of nitrate (NO_3^--N) or nitrite (NO_2^--N) under aerobic conditions [78]. This distribution is supported by a high adsorption capacity (24.56 mg/g) and a removal efficiency of 35.25% at this neutral pH, with post-adsorption SEM and EDS measurements indicating a nitrogen content of 9.28 wt%.

Multilayer adsorption further increases nitrogen trapping on the heterogeneous surfaces of the SPO, which has a porous structure as seen in SEM images. Osmonation enhances the porosity and availability of reactive sites on the biochar and facilitates the subsequent adsorption of other nitrogen forms, especially organic nitrogen, which can form hydrogen bonds with -OH and -COOH groups. As demonstrated in contact time studies, the adsorption capacity increases significantly to 32.56 mg/g at longer contact times, indicative of a two-phase process in which initial rapid chemisorption is followed by a slower multilayer buildup in the internal pores of SPO [79]. The XGB model (Fig. 9d) and SHAP analysis (Fig. 10) reinforce this mechanism. Ads_dos (mean SHAP = 7.736, -40 to +70) drives chemisorption site availability, N_con (mean SHAP = 3.607, -30 to +60) enhances the driving force for multilayer adsorption and Time (mean SHAP = 2.401, -20 to +30) supports diffusion. In contrast, pH (mean SHAP = 2.612, -20 to +30) optimizes charge interactions at pH 7.

The concentration study reveals that the removal efficiency peaks at 93.67% at a nitrogen concentration of 27.87 mg/L. This suggests that lower nitrogen concentrations facilitate the efficient formation of a multilayer structure, as the active sites remain largely unsaturated, a factor crucial for increasing adsorption efficiency [80]. The role of surface heterogeneity is critical, as illustrated by the use of the Elovich kinetic model and the Freundlich isotherm to represent the diverse landscape of the SPO. In addition, ozonation-induced changes, such as the appearance of new FTIR peaks at 1255 cm-1 (C-O) and 878 cm-1 (C-H), contribute significantly to this diversity and support both chemisorption and multilayer adsorption mechanisms [81].

Pore diffusion is critical to the overall adsorption process, and the porous structure of the SPO enables nitrogen species to penetrate deeper into the biochar matrix. This property is supported by the persistent nitrogen uptake observed during the initial contact period in the studies. Overall, the interactions and mechanisms underlying nitrogen adsorption by SPO underscore its promise as an efficient adsorbent, driven by a combination of improved surface chemistry and structural properties that enable optimal nitrogen removal from wastewater [82,83].

3.11. Applicability, reusability, cost analysis and scalability

While the current study demonstrates promising TN adsorption performance of ozone-modified acacia wood sawdust biochar (SPO) under optimized lab-scale conditions (pH 7, 0.2–0.6 g/50 mL dosage, 270 min contact time), the experiments were limited to batch-mode tests at small volumes (50 mL) with simulated and filtered real swine wastewater (initial TN: 27–279 mg/L). This constrains direct claims of field-scale applicability, as factors like continuous flow dynamics, variable wastewater matrices (e.g., fluctuating COD/N ratios), and long-term column clogging were not evaluated. To bridge this gap, future work should incorporate fixed-bed column studies and pilot trials at swine farms, potentially integrating SPO into post-biogas polishing units for enhanced nutrient recovery. Preliminary modeling suggests SPO could achieve 40–50% TN reduction in full-scale anaerobic-aerobic systems, mitigating eutrophication risks while producing value-added fertilizer precursors [84].

Building upon the optimized adsorption conditions and mechanistic insights established in this study, future research will focus on the recovery and valorization of adsorbed nitrogen and ammonia from SPO to promote a circular economy in livestock wastewater management. Specifically, the nutrient content fixed within post-adsorption SPO (e.g., NH_4^+-N, NO_3^--N, and organic nitrogen forms) will be quantified using established analytical methods, including the Kjeldahl procedure, Devarda's alloy reduction, and advanced spectroscopic techniques. This will enable a precise assessment of nitrogen bioavailability and transformation dynamics under soil incubation conditions, including microbial-mediated mineralization and slow-release kinetics in degraded soils. Field trials will evaluate SPO's efficacy as a biofertilizer for remediating nutrient-depleted agricultural lands, comparing its performance with synthetic fertilizers in terms of soil fertility enhancement, crop yield improvement, and reductions in chemical fertilizer inputs (estimated at 30–50% nitrogen savings). These efforts address the urgency of nitrogen removal from pig wastewater, which, if unmanaged, exacerbates environmental degradation through eutrophication, biodiversity loss and air pollution from ammonia volatilization. By integrating recovery, the approach yields broader benefits: environmentally, it mitigates reactive nitrogen emissions that exceed planetary boundaries and reduces fossil-based fertilizer demand.

The recyclability of ozone-modified acacia wood sawdust biochar (SPO) for total nitrogen (TN) adsorption from pig wastewater was assessed over five consecutive adsorption-desorption cycles, as illustrated in Fig. 12. The initial adsorption capacity in cycle one was recorded at 32.57 mg/g, reflecting optimal surface functionality and porosity. Subsequent cycles demonstrated a progressive decline in capacity, with values of 28.53 mg/g (87.60% retention relative to cycle 1), 24.22 mg/g (74.36% retention), 21.65 mg/g (66.47% retention), and 17.35 mg/g (53.27% retention) in cycles 2 through 5, respectively. This attenuation is likely attributable to incomplete desorption of bound nitrogen species, gradual deactivation of oxygen-containing functional groups (-OH and -COOH) during regeneration and minor pore blockage from residual organic matter in the wastewater matrix, consistent with observations in similar modified biochars. Despite the observed reduction, SPO retained over 50% of its initial capacity after five cycles, underscoring its moderate reusability and potential for cost-effective deployment in multi-cycle wastewater treatment systems. These results indicate that SPO is viable for 3–4 practical cycles before significant performance loss, with implications for scalable applications in intensive livestock operations, where spent adsorbent could be repurposed as a nutrient-rich soil amendment to promote circular economy practices. Future studies should explore advanced regeneration techniques, such as thermal or alkaline desorption, to further extend cycle life and enhance economic feasibility.

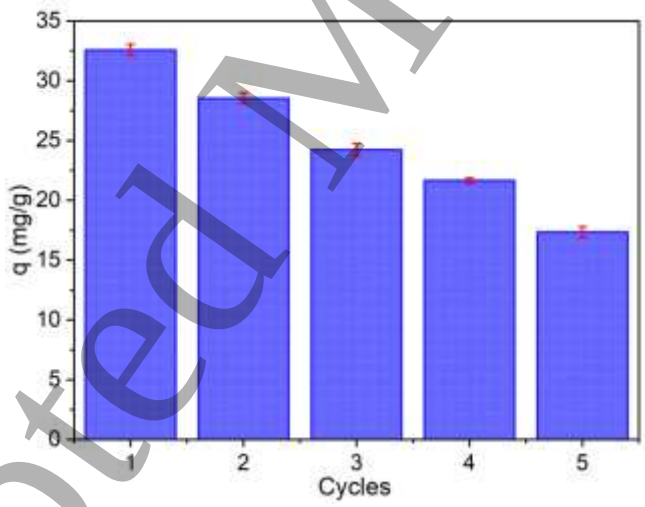

Fig. 12. The recyclability of the SPO for TN adsorption

From an economic perspective, SPO production is highly cost-effective, leveraging abundant acacia sawdust waste (Vietnam's annual output: ~2 million tons). Pyrolysis at 600°C requires ~0.5–1 kWh/kg energy (~0.05 USD/kg), ozonation adds ~0.10 USD/kg (10 g/h generator), yielding a total cost of 0.15–0.25 USD/kg—50–80% lower than commercial zeolite (0.5–1 USD/kg) or activated carbon (1–2 USD/kg) [85]. This cost profile is consistent with recent studies on low-cost agricultural waste adsorbents, such as groundnut shell - requiring minimal preprocessing (drying only) and available at near-zero acquisition cost in rural settings [86] - and walnut shell, which demonstrated economic feasibility through regeneration (up to 4 cycles with HCl) and pilot-scale design with payback within 2 years [87]. These benchmarks confirm SPO's technical and economic viability for decentralized, real-world nutrient recovery from high-strength livestock wastewater. Scalability is feasible via decentralized, low-tech pyrolyzers (e.g., drum-based systems

processing 100–500 kg/day), reducing transport emissions by 40–60% compared to imported adsorbents. Life-cycle assessment indicates a payback period of 1–2 years in mid-scale swine operations (500–2000 heads), with net environmental benefits from N recovery (avoiding ~200 kg eutrophication potential/ha) outweighing production emissions [88]. Challenges include seasonal feedstock variability and O_3 generator maintenance, which are addressable through hybrid solar-powered systems.

The comparative analysis of SPO with other adsorbents for ammonium nitrogen (NH_4^+-N) or total nitrogen (TN) removal from swine wastewater, as summarized in Table 3, reveals SPO's competitive performance in terms of adsorption capacity (32.38 mg/g for TN) and removal efficiency (46.39%), balanced by its low production cost (0.15–0.25 USD/kg) and sustainability derived from waste biomass. In contrast, magnesite-modified biochar exhibits superior capacity (138.39 mg/g for NH_4^+-N) and efficiency (97.5%), attributed to enhanced ion exchange resulting from mineral doping; however, its reliance on mining tailings raises environmental concerns and limits scalability in resource-constrained regions [89]. Rice husk biochar (RHB) shows a wide capacity range (2.8–137.3 mg/g for NH_4^+-N) with comparable efficiency (43.2%), but lacks the surface oxygenation of SPO, resulting in weaker interactions with organic nitrogen species [84]. Biochar pellets from pig manure achieve high efficiency (92.2%) despite a low capacity (2.94 mg/g for NH_4^+-N), potentially due to their macroporous structure. However, microbial contamination risks from the manure feedstock undermine their safety for wastewater reuse [27]. Natural zeolite (clinoptilolite) offers moderate capacity (0.7–65.3 mg/g for NH_4^+) and efficiency (64–79%), with good reusability, but its higher cost (0.5–1.0 USD/kg) and susceptibility to matrix interference in complex swine effluents make it less economical than SPO [74]. Synthesized zeolite from fly ash matches SPO's capacity (32.16 mg/g for NH_4^+) at a slightly higher cost (0.2–0.4 USD/kg), yet requires energy-intensive synthesis, contrasting SPO's simple pyrolysis-ozonation process [26]. Activated carbon (AC) demonstrates exceptional capacity (up to 396.9 mg/g for NH_3 in air matrices) and efficiency (81–92%), but its prohibitive commercial cost (1–2 USD/kg) and high activation energy render it unsuitable for large-scale agricultural applications [34,90]. Overall, SPO stands out for its optimal trade-off among performance, cost-effectiveness, and eco-friendliness, positioning it as a viable alternative for decentralized swine wastewater treatment in developing contexts, warranting further pilot-scale validation to confirm its real-world advantages.

Table 3. Comparison of SPO with selected adsorbents for NH_4^+-N/TN removal from swine wastewater

Adsorbent	Material source	Max. adsorption capacity (mg/g)	Removal efficiency (%)	Estimated cost (USD/kg)	Reference
SPO Biochar (this study)	Ozone-modified acacia sawdust	32.38 (TN)	46.39	0.15–0.25	This study
Rice Husk Biochar (RHB)	Rice husk pyrolysis	2.8–137.3 (NH_4^+-N)	43.2 (NH_3 reduction)	Low (waste-derived)	[89]
Natural Zeolite	Clinoptilolite	0.7–65.3 (NH_4^+)	23.3 (NH_3 reduction) / 64–79	0.5–1.0	[84]
Magnesite-Modified Biochar	Rice straw + tailings	138.39 (NH_4^+)	97.5	Extremely low (<0.1)	[74]
Biochar Pellet (pig manure)	Pig manure + biochar	2.94 (NH_4^+-N)	92.2	Low (waste-based)	[27]
Synthesized Zeolite	Fly ash-derived	32.16 (NH_4^+)	64–79	0.2–0.4	[26]
Activated Carbon (AC)	Wood/sawdust (KOH-activated)	Up to 396.9 (NH_3, air matrix)	81–92 (TOC/NH_4^+, synthetic)	1–2 (commercial); 0.22–2.73 (produced)	[34,90]

Conclusion

This study identified ozone-modified acacia wood sawdust biochar (SPO) as an efficient and sustainable solution for nitrogen removal from pig wastewater. At pH 7, SPO dosage of 0.2 g/50 mL and a 270-minute contact time, SPO achieved the highest adsorption capacity of 32.38 mg/g and a removal efficiency of 46.39% at an initial TN of 279 mg/L. The enhanced oxygen content (22.28 wt%) and functional groups (-OH, -COOH) facilitated chemisorption and multilayer adsorption, validated by pseudo-second-order (R^2 = 0.9310) and Freundlich (R^2 = 0.9612) models. Machine learning, particularly the XGB model (R^2 = 0.998), accurately predicted removal efficiency, with SHAP analysis highlighting adsorbent dosage (mean SHAP = 7.736) and nitrogen concentration (mean SHAP = 3.607) as critical factors. These findings highlight the potential of SPO for scalable

wastewater treatment, offering a data-driven, environmentally friendly approach to mitigating nitrogen pollution from intensive livestock production, with implications for broader environmental management strategies. With a production cost of only 0.15–0.25 USD/kg and a 53.27% adsorption capacity (17.35 mg/g) retained after five reuse cycles, SPO offers a sustainable and economically viable alternative to conventional adsorbents, supporting its integration into decentralized nutrient recovery systems in intensive pig farming.

Looking ahead, this work lays the foundation for an integrated livestock wastewater treatment system that incorporates nutrient recovery, transforming adsorbed nitrogen into biofertilizers for soil remediation and reduced chemical fertilizer dependency. The urgency of removal is underscored by its role in preventing severe environmental impacts, such as exceeding planetary nitrogen boundaries and contributing to global eutrophication, while recovery delivers substantial economic advantages.

Acknowledgment

This research is supported by the scientific and technological task funded by Thai Nguyen University, conducted from 2024, under grant number ĐH2024-NV-01.

Data availability

Datasets were generated or analyzed during the current study

Declaration of competing interest

The authors declare that they have no known competing financial interests or personal relationships that could have appeared to influence the work reported in this paper.

References

[1] Qian G, Chen J, Luo L, Zhang H, Chen W, Gao Z, Yin S and Tsiakaras P 2020 Novel Bifunctional V₂O₃ Nanosheets Coupled With N-Doped-Carbon Encapsulated Ni Heterostructure for Enhanced Electrocatalytic Oxidation of Urea-Rich Wastewater *ACS Appl. Mater. Interfaces* **12** 38061–9

[2] Kowitwiwat A and Sampanpanish P 2020 Phytostabilization of Arsenic and Manganese in Mine Tailings Using Pennisetum Purpureum Cv. Mott Supplemented With Cow Manure and Acacia Wood-Derived Biochar *Heliyon* **6** e04552

[3] Du D, Zhou J, Zhang K and Zhi S 2022 Seasonal Pollution Characteristics of Antibiotics on Pig Farms of Different Scales *Int. J. Environ. Res. Public Health* **19** 8264

[4] Campos E G de, Almeida O G G de, Martinis B S De and Martinis E C P De 2021 Cocaine Esterase Occurrence in Global Wastewater Microbiomes and Potential for Biotransformation of Novel Psychoactive Substances *Environ. Microbiol. Rep.* **14** 96–109

[5] Zheng Z, Liao C, Chen Y, Ming T, Jiao L, Kong F M, Su X and Xu J 2024 Revealing the Functional Potential of Microbial Community of Activated Sludge for Treating Tuna Processing Wastewater Through Metagenomic Analysis *Front. Microbiol.* **15** 1430199

[6] Boro D, Chirania M, Verma A K, Chettri D and Verma A K 2025 Comprehensive approaches to managing emerging contaminants in wastewater: identification, sources, monitoring and remediation *Environ. Monit. Assess.* **197** 456

[7] Ijaz M U, Akbar A, Eman R, Hayat M F, Naz H and Ashraf A 2025 Mitigating Nutrient Pollution from Livestock Manure: Strategies for Sustainable Management BT - Agricultural Nutrient Pollution and Climate Change: Challenges and Opportunities *Agricultural Nutrient Pollution and Climate Change* ed N Hussain, C-Y Hung and L Wang (Cham: Springer Nature Switzerland) pp 165–87

[8] Zhi S, Shen S, Zhou J, Ding G and Zhang K 2020 Systematic Analysis of Occurrence, Density and Ecological Risks of 45 Veterinary Antibiotics: Focused on Family Livestock Farms in Erhai Lake Basin, Yunnan, China *Environ. Pollut.* **267** 115539

[9] Ayinde W B, Ikumi D and Basitere M 2025 Veterinary antibiotic removal from poultry slaughterhouse (PSH) wastewater: a mini-review of environmental nanoremediation techniques *Environ. Technol. Rev.* **14** 359–70

[10] Liu X, Li G, Chen C, Zhang X, Zhou K and Long X 2022 Banana Stem and Leaf Biochar as an Effective Adsorbent for Cadmium and Lead in Aqueous Solution *Sci. Rep.* **12** 1584

[11] Chen W and Kim T 2025 A mini-review on performance metrics for electrochemically mediated ammonia recovery from wastewater *Environ. Sci. Water Res. Technol.*

[12] Jiang D, Wang H, Cao X, Wang R, Dai Z, Zhang W, Abbasi H N, Li B, Wang X and Dai H 2025 Advancements and Future Perspectives in Biological Nitrogen and Phosphorus Removal Coupled Resource Recovery Processes *Water, Air, Soil Pollut.* **236** 488

[13] Zhang Y, Zhang S, Lin Y, Wu S, Li X and Yang C 2025 Simultaneous removal of heavy metals and antibiotics from anaerobically digested swine wastewater via functionalized covalent organic frameworks *Environ. Res.* **272** 121152

[14] Altaf R, Liu D, Jaafarzadeh N, Zou J, Zhou Y, Wu B, Lin X and Liu D 2025 Phosphorus removal and recovery from livestock wastewater by using modified zirconium-lanthanum magnetite *J. Water Process Eng.* **71** 107385

[15] Wang S, Zhao H, Liu J, Wang X, Li J, Shi E, Wang C, Yang J and Zhang Z 2023 A Study on and Adsorption Mechanism of Ammonium Nitrogen by Modified Corn Straw Biochar *R. Soc. Open Sci.* **10** 221535

[16] Ministry of Agriculture and Rural Development of Vietnam 2023 *Annual Report on Forestry and Wood Processing Sector*

[17] Rajapaksha A U, Chen S S, Tsang D C W, Zhang M, Vithanage M, Mandal S, Gao B, Bolan N S and Ok Y S 2016 Engineered/designer biochar for contaminant removal/immobilization from soil and water: Potential and implication of biochar modification *Chemosphere* **148** 276–91

[18] Liu W-J, Jiang H and Yu H-Q 2015 Development of Biochar-Based Functional Materials: Toward a Sustainable Platform Carbon Material *Chem. Rev.* **115** 12251–85

[19] Wang B, Lehmann J, Hanley K, Hestrin R and Enders A 2015 Adsorption and desorption of ammonium by maple wood biochar as a function of oxidation and pH

Chemosphere **138** 120–6

[20] Khater E S, Bahnasawy A, Hamouda R, Sabahy A, Abbas W and Morsy O M 2024 Biochar production under different pyrolysis temperatures with different types of agricultural wastes *Sci. Rep.* **14** 1–8

[21] Kharel G, Sacko O, Feng X, Morris J R, Phillips C L, Trippe K M, Kumar S and Lee J W 2019 Biochar Surface Oxygenation by Ozonization for Super High Cation Exchange Capacity *Acs Sustain. Chem. Eng.* **7** 16410–8

[22] Zhang W, Chen R, Li J, Huang T, Wu B, Ma J, Wen Q, Tan J and Huang W 2023 Synthesis optimization and adsorption modeling of biochar for pollutant removal via machine learning *Biochar* **5** 25

[23] Claude B M J and Sibali L L 2024 Application of machine learning for environmentally friendly advancement: exploring biomass-derived materials in wastewater treatment and agricultural sector − a review *J. Environ. Sci. Heal. Part A* **59** 606–21

[24] Mansour M, Bassyouni M, Abdel-Kader R F, Elhenawy Y, Said L A and Abdel-Hamid S M S 2024 Artificial Intelligence for Predicting the Performance of Adsorption Processes in Wastewater Treatment: A Critical Review BT - Engineering Solutions Toward Sustainable Development *Engineering Solutions Toward Sustainable Development* ed A M Negm, R Y Rizk, R F Abdel-Kader and A Ahmed (Cham: Springer Nature Switzerland) pp 153–73

[25] Zhang H, Voroney R P and Price G W 2015 Effects of temperature and processing conditions on biochar chemical properties and their influence on soil C and N transformations *Soil Biol. Biochem.* **83** 19–28

[26] Eldeeb T M, Aigbe U O, Ukhurebor K E, Onyancha R B, El-Nemr M A, Hassaan M A, Ragab S, Osibote O A and El Nemr A 2024 Adsorption of methylene blue (MB) dye on ozone, purified and sonicated sawdust biochars *Biomass Convers. Biorefinery* **14** 9361–83

[27] Thommes M, Kaneko K, Neimark A V, Olivier J P, Rodriguez-Reinoso F, Rouquérol J and Sing K S W 2015 Physisorption of Gases, With Special Reference to the Evaluation of Surface Area and Pore Size Distribution (IUPAC Technical Report) *Pure Appl. Chem.* **87** 1051–69

[28] Vietnam government 2000 *TCVN 6638:2000 - Water quality - Determination of nitrogen - Catalytic digestion after reduction with devarda\'s alloy*

[29] Schossler R T, Ojo S, Jiang Z, Hu J and Yu X 2024 A novel interpretable machine learning model approach for the prediction of TiO2 photocatalytic degradation of air contaminants *Sci. Rep.* **14** 1–15

[30] Vakarelska E, Nedyalkova M, Vasighi M and Simeonov V 2022 Persistent organic pollutants (POPs) - QSPR classification models by means of Machine learning strategies *Chemosphere* **287** 132189

[31] Braghiroli F L, Bouafif H, Hamza N, Bouslimi B, Neculita C M and Koubaa A 2018 The Influence of Pilot-Scale Pyro-Gasification and Activation Conditions on Porosity Development in Activated Biochars *Biomass and Bioenergy* **118** 105–14

[32] Shang X, Hung C, Husk B, Orsat V and Whalen J K 2022 Wood-Based Biochar for Small Fruit Production in Southern Quebec, Canada *Can. J. Soil Sci.* **102** 89–96

[33] Wani O A, Akhter F, Kumar S S, Babu S, Kanth R H, Mir S A, Mahdi S S, Malik A R, Bangroo S A, Gaafar A Z, Popescu S M and Rathore S S 2023 Mitigating Soil Erosion Through Biomass-Derived Biochar: Exploring the Influence of Feedstock Types and Pyrolysis Temperature *Land* **12** 2111

[34] Joseph S, Kammann C, Shepherd J G, Conte P, Schmidt H, Hagemann N, Rich A M, Marjo C E, Allen J, Munroe P, Mitchell D R G, Donne S W, Spokas K A and Gräber E R 2018 Microstructural and Associated Chemical Changes During the Composting of a High Temperature Biochar: Mechanisms for Nitrate, Phosphate and Other Nutrient Retention and Release *Sci. Total Environ.* **618** 1210–23

[35] Amin A E-E A Z 2023 Effects of Saline Water on Soil Properties and Red Radish Growth in Saline Soil as a Function of Co-Applying Wood Chips Biochar With Chemical Fertilizers *BMC Plant Biol.* **23** 382

[36] He Z, Liu S, Zhao W, Yin M, Jiang M and Bi D 2022 Comparative Assessment of Proportions of Urea in Blend for Nitrogen-Rich Pyrolysis: Characteristics and Distribution of Bio-Oil and Biochar *Acs Omega* **8** 1232–9

[37] Lawrinenko M, Laird D A, Johnson R L and Jing D 2016 Accelerated Aging of Biochars: Impact on Anion Exchange Capacity *Carbon N. Y.* **103** 217–27

[38] Li Y, Guan J, Xu B, Wang G, Lin G, Li D, Gao Y and Zhao J 2023 Molecular Insights Into Mercury Sequestration by the Sulfate and Biochar Combined Application Strategy Guide Pollution Treatments *Acs Es&t Eng.* **4** 761–70

[39] Huff M, Marshall S, Saeed H A and Lee J W 2018 Surface Oxygenation of Biochar Through Ozonization for Dramatically Enhancing Cation Exchange Capacity *Bioresour. Bioprocess.* **5** 18

[40] Fan B, Jia L, Li B, Yao Y, Huo R, Zhao R, Qiao X and Jin Y 2018 Study on the Effects of the Pyrolysis Atmosphere on the Elemental Mercury Adsorption Characteristics and Mechanism of Biomass Char *Energy & Fuels* **32** 6869–78

[41] Zhang M, Song G, Gelardi D L, Huang L, Khan E, Xu G, Parikh S J and Kim K-H 2020 Evaluating Biochar and Its Modifications for the Removal of Ammonium, Nitrate, and Phosphate in Water *Water Res.* **186** 116303

[42] Lafdani E K, Laurén A, Cvetković J, Pumpanen J, Saarela T and Palviainen M 2021 Nitrogen Recovery From Clear-Cut Forest Runoff Using Biochar: Adsorption–Desorption Dynamics Affected by Water Nitrogen Concentration *Water Air Soil Pollut.* **232** 432

[43] Wu X, Ye M, Wang J, Wu F, Liu C, Li Z, Dai-yan L and Yang R 2023 Adsorption Characteristics and Mechanism of Ammonia Nitrogen and Phosphate From Biogas Slurry by Ca2+-Modified Soybean Straw Biochar *PLoS One* **18** e0290714

[44] Yin W, Zhang W, Zhao C and Xu J 2019 Evaluation of Removal Efficiency of Ni(II) and 2,4-DCP Using in Situ Nitrogen-Doped Biochar Modified With Aquatic Animal Waste *Acs Omega* **4** 19366–74

[45] Tu P, Zhang G, Cen Y, Huang B, Li J, Li Y, Deng L and Yuan H 2023 Effect of Modified Biochar Prepared by Co-pyrolysis of MgO on Phosphate Adsorption Performance and Seed Germination *Chempluschem* **89** e202300305

[46] Jiang W, Xing Y, Zhang L, Guo X, Lu Y, Yang M, Wang J and Wei G 2020 Polyethylenimine-modified Sugarcane Bagasse Cellulose as an Effective Adsorbent for Removing Cu(II) From Aqueous Solution *J. Appl. Polym. Sci.* **138** 49830

[47] Chen H, Han X and Liu Y 2021 Gaseous Hydrogen Sulfide Removal Using Macroalgae Biochars Modified Synergistically by H₂SO₄/H₂O₂ *Chem. Eng. Technol.* **44** 698–709

[48] Fard F A, Yengejeh R J and Ghaeni M 2019 Efficiency of Microalgae Scenedesmus in the Removal of Nitrogen From Municipal Wastewaters *Iran. J. Toxicol.* **13** 1–6

[49] Amari A, Noreen A, Osman H, Sammen S S, Al-Ansari N and Salman H M 2023 Investigation of the Viable Role of Oil Sludge-Derived Activated Carbon for Oily Wastewater Remediation *Front. Environ. Sci.* **11** 1–13

[50] He S, Ding L, Pan Y, Hu H, Ye L and Ren H 2018 Nitrogen Loading Effects on Nitrification and Denitrification With Functional Gene Quantity/Transcription Analysis in Biochar Packed Reactors at 5 °C *Sci. Rep.* **8** 9844

[51] Qiu J, Li X, Peng Y and Jiang H 2022 Advanced nitrogen removal from landfill leachate via a two-stage combined process of partial nitrification-Anammox (PNA) and partial denitrification-Anammox (PDA) *Sci. Total Environ.* **810** 151186

[52] Ling Y, Yan G, Wang H, Dong W, Wang H, Chang Y, Chang M and Li C 2021 Release Mechanism, Secondary Pollutants and Denitrification Performance Comparison of Six Kinds of Agricultural Wastes as Solid Carbon Sources for Nitrate Removal *Int. J. Environ. Res. Public Health* **18** 1232

[53] Pan F, Huang F, Wang Y and Zhu H 2024 Effects of Rice Husk Biochar Attachment Biofilm With Microorganisms on Nitrogen Removal of Digested Swine Wastewater *Bioresources* **19** 6264–80

[54] Kaetzl K, Lübken M, Nettmann E, Krimmler S and Wichern M 2020 Slow Sand Filtration of Raw Wastewater Using Biochar as an Alternative Filtration Media *Sci. Rep.* **10** 1229

[55] Janyasupab P and Jampeetong A 2022 Performance of Porous Substrates for Domestic Wastewater Treatment Under Prolonged Hydraulic Retention Time *Appl. Environ. Res.* **44** 45–58

[56] Saarela T, Lafdani E K, Laurén A, Pumpanen J and Palviainen M 2020 Biochar as Adsorbent in Purification of Clear-Cut Forest Runoff Water: Adsorption Rate and Adsorption Capacity *Biochar* **2** 227–37

[57] Ahmadvand M, Soltani J, Garmdareh S E H and Varavipour M 2018 The Relationship Between the Characteristics of Biochar Produced at Different Temperatures and Its Impact on the Uptake of NO3 - -N *Environ. Heal. Eng. Manag.* **5** 67–75

[58] Palviainen M, Berninger F, Bruckman V J, Köster K, Assumpção C R M de, Aaltonen H, Makita N, Mishra A, Kulmala L, Adamczyk B, Zhou X, Heinonsalo J, Köster E and Pumpanen J 2018 Effects of Biochar on Carbon and Nitrogen Fluxes in Boreal Forest Soil *Plant Soil* **425** 71–85

[59] Yao J, Wang Z, Liu M, Bai B and Zhang C 2023 Nitrate-Nitrogen Adsorption Characteristics and Mechanisms of Various Garden Waste Biochars *Materials (Basel).* **16** 5726

[60] Liu D, Cui C, Wu Y, Chen H, Geng J and Xia J 2018 Highly Efficient Removal of Ammonia Nitrogen From Wastewater by Dielectrophoresis-Enhanced Adsorption *PeerJ* **6** e5001

[61] Koohzad E, Jafari D and Esmaeili H 2019 Adsorption of Lead and Arsenic Ions From Aqueous Solution by Activated Carbon Prepared From Tamarix Leaves *Chemistryselect* **4** 12356–67

[62] Song H, Wang J, Garg A, Lin X, Zheng Q and Sharma S 2019 Potential of Novel Biochars Produced From Invasive Aquatic Species Outside Food Chain in Removing Ammonium Nitrogen: Comparison With Conventional Biochars and Clinoptilolite *Sustainability* **24** 7136

[63] Zuo J, Zhao T, Yang S, Xia Z, Tan C, Li J and Wang Y 2023 Enhanced Treatment of Potato Starch Wastewater Using Chitosan-Modified Biochar Film Adsorption Coupled With Ultrafiltration *Coatings* **13** 2017

[64] Devasena S S, Padmavathy P, Manimekalai D and Shakila R J 2020 Assessment of Fish Scale Biosorbent in the Treatment of Seafood Processing Plant Wastewater *J. Chem. Technol. Biotechnol.* **96** 723–31

[65] Teğin İ, Öc S and Saka C 2024 Adsorption of Copper (II) From Aqueous Solutions Using Adsorbent Obtained With Sodium Hydroxide Activation of Biochar Prepared by Microwave Pyrolysis *Biomass Convers. Biorefinery* **15** 6805–16

[66] Li D, Liu Z, Armaghani D J, Xiao P and Zhou J 2022 Novel Ensemble Intelligence Methodologies for Rockburst Assessment in Complex and Variable Environments *Sci. Rep.* **12** 1844

[67] García R T M, Céspedes-López M F and Perez-Sanchez V R 2022 Housing Price Prediction Using Machine Learning Algorithms in COVID-19 Times *Land* **11** 2100

[68] Briggs E, Kamps M de, Hamilton W, Johnson O, McInerney C and Neal R D 2022 Machine Learning for Risk Prediction of Oesophago-Gastric Cancer in Primary Care: Comparison With Existing Risk-Assessment Tools *Cancers (Basel).* **14** 5023

[69] Yang Q, Wanlin L and Maofeng W 2024 Machine Learning Derived Model for the Prediction of Bleeding in Dual Antiplatelet Therapy Patients *Front. Cardiovasc. Med.* **11** 1402672

[70] Indu I, Abba S and Boukari S 2024 International Journal of Research Publication and Reviews A Review on Analysis of Stock Market Prediction Using Supervised Machine Learning Algorithms *Int. J. Res. Publ. Rev.* **5** 295–8

[71] Abdu A M, Mokji M M and Sheikh U U 2020 Machine Learning for Plant Disease Detection: An Investigative Comparison Between Support Vector Machine and Deep Learning *Iaes Int. J. Artif. Intell.* **9** 670

[72] Chicco D and Jurman G 2020 The Advantages of the Matthews Correlation Coefficient (MCC) Over F1 Score and Accuracy in Binary Classification Evaluation *BMC Genomics* **21** 6

[73] Zhang Y, Xu J, Zhang C, Zhang X, Yuan X, Ni W, Zhang H, Zheng Y and Zhao Z 2024 Community Screening for Dementia Among Older Adults in China: A Machine Learning-Based Strategy *BMC Public Health* **24** 1206

[74] Li X 2023 Lung Cancer Risk Prediction and Feature Importance Analysis With Machine Learning Algorithm *Appl. Comput. Eng.* **19** 205–10

[75] Razali N, Ismail S and Mustapha A 2020 Machine Learning Approach for Flood Risks Prediction *Iaes Int. J. Artif. Intell.* **9** 73

[76] Yao Y, Gao B, Zhang M, Inyang M and Zimmerman A R 2012 Effect of biochar amendment on sorption and leaching of nitrate, ammonium, and phosphate in a sandy soil *Chemosphere* **89** 1467–71

[77] Yin Q, Zhang B, Wang R and Zhao Z 2017 Biochar as an adsorbent for inorganic nitrogen and phosphorus removal from water: a review. *Environ. Sci. Pollut. Res. Int.* **24** 26297–309

[78] Cho J and Kim S-J 2000 Increase in Bacterial Community Diversity in Subsurface Aquifers Receiving Livestock

Wastewater Input *Appl. Environ. Microbiol.* **66** 956–65

[79] Fang C, Zhang T, Li P, Jiang R F and Wang Y C 2014 Application of magnesium modified corn biochar for phosphorus removal and recovery from swine wastewater *Int. J. Environ. Res. Public Health* **11** 9217–37

[80] Li S, Tasnady D, Skelley S, Calderón B and Jiang S 2024 Enhancing Organic Contaminant Removal From Wool Scouring Wastewater Using Chemically Modified Biochars *C – J. Carbon Res.* **10** 6

[81] Lopez M A R, Ferreira G M D, Figueiredo M T D, Ferreira G M D, Franca J R, Penido E S, Ribeiro-Soares J, Longuinhos R and Mageste A B 2025 Mechanisms of Phenol Adsorption on Banana Leaves and Coffee Husk Biochars *Acs Omega* **10** 15989–6005

[82] Jha S, Gaur R, Shahabuddin S and Tyagi I 2023 Biochar as Sustainable Alternative and Green Adsorbent for the Remediation of Noxious Pollutants: A Comprehensive Review *Toxics* **11** 117

[83] Yang H I, Lou K, Rajapaksha A U, Ok Y S, Anyia A O and Chang S X 2018 Adsorption of ammonium in aqueous solutions by pine sawdust and wheat straw biochars *Environ. Sci. Pollut. Res.* **25** 25638–47

[84] Tang H, Xu X, Wang B, Lv C and Shi D 2020 Removal of Ammonium from Swine Wastewater Using Synthesized Zeolite from Fly Ash *Sustainability* **12**

[85] Somashekara D and Mulky L 2023 Sequestration of Contaminants from Wastewater: A Review of Adsorption Processes *ChemBioEng Rev.* **10** 491–509

[86] Das A, Bar N and Das S K 2023 Adsorptive removal of Pb(II) ion on Arachis hypogaea's shell: Batch Experiments, statistical, and GA modeling *Int. J. Environ. Sci. Technol.* **20** 537–50

[87] Banerjee M, Bar N and Das S K 2021 Cu(II) Removal From Aqueous Solution Using The Walnut Shell: Adsorption Study, Regeneration Study, Plant Scale-Up Design, Economic Feasibility, Statistical, and GA-ANN Modeling *Int. J. Environ. Res.* **15** 875–91

[88] Arena N, Lee J and Clift R 2016 Life Cycle Assessment of activated carbon production from coconut shells *J. Clean. Prod.* **125** 68–77

[89] Lorenz K and Lal R 2014 Biochar application to soil for climate change mitigation by soil organic carbon sequestration *J. Plant Nutr. Soil Sci.* **177** 651–70

[90] Bado V B and Bationo A 2018 Chapter One - Integrated Management of Soil Fertility and Land Resources in Sub-Saharan Africa: Involving Local Communities vol 150, ed D L B T-A in A Sparks (Academic Press) pp 1–33